KIF2A Regulates the Development of Dentate Granule Cells and Postnatal Hippocampal Wiring

Noriko Homma[1#], Ruyun Zhou[1], Muhammad Imran Naseer[2], Adeel G. Chaudhary[2], Mohammed H. Al-Qahtani[2], and Nobutaka Hirokawa[1&2]*

[1]Department of Cell Biology and Anatomy, Graduate School of Medicine, the University of Tokyo, Tokyo 113-0033, Japan, [2]Center of Excellence in Genomic Medicine Research, King Abdulaziz University, Jeddah, 21589, Saudi Arabia

*Corresponding author: Nobutaka Hirokawa; Department of Cell Biology and Anatomy, Graduate School of Medicine, the University of Tokyo, 7-3-1, Hongo, Bunkyo-ku, Tokyo 113-0033, Japan hirokawa@m.u-tokyo.ac.jp

[#]Present address: Department of Lifescience, National College of Nursing, Tokyo 204-8575, Japan.

Major subject: Neuroscience and Cell Biology

Running title: Postnatal KIF2A Regulates Hippocampal Wiring

Number of Figures and Videos: **7** Figures, 5 Figure supplements, and 3 Videos

Key words: KIF2A /dentate granule cell/ postnatal hippocampal wiring/ dentate granule cell/ dendro-axonal determination / temporal lobe epilepsy

Abstract

Kinesin super family protein 2A (KIF2A), an ATP-dependent microtubule (MT) destabilizer, regulates cell migration, axon elongation, and pruning in the developing nervous system. KIF2A mutations have recently been identified in patients with malformed cortical development. However, postnatal KIF2A is continuously expressed in the hippocampus, in which new neurons are generated throughout an individual's life in established neuronal circuits. In this study, we investigated KIF2A function in the postnatal hippocampus by using tamoxifen-inducible *Kif2a* conditional knockout (*Kif2a*-cKO) mice. Despite exhibiting no significant defects in neuronal proliferation or migration, *Kif2a*-cKO mice showed signs of an epileptic hippocampus. In addition to mossy fiber sprouting, the *Kif2a*-cKO dentate granule cells (DGCs) showed *dendro-axonal conversion*, leading to the growth of many aberrant overextended dendrites that eventually developed axonal properties. These results suggested that postnatal KIF2A is a key length regulator of DGC developing neurites and is involved in the establishment of precise postnatal hippocampal wiring.

Introduction

In the mammalian nervous system, kinesin super family proteins (KIFs) play a crucial role in intracellular transport, microtubule (MT) dynamics, and signal transduction and, hence, are key players in brain function, development, and disease [1, 2]. KIF2A belongs to the kinesin-13 family (M-kinesin: internal motor domain family) [3-5], which destabilizes MTs in an ATP-dependent manner [6-8]. In the early stages of the developing murine nervous system, KIF2A controls neurite elongation by regulating MT dynamics at neuronal growth cones and plays a crucial role in neuronal migration, axonal elongation and axon pruning *in vivo* [9-12].

Recently, studies of KIF2A function in humans have primarily focused on cortical development because KIF2A mutations in residues Ser317 and His321 have been identified in patients with malformed cortical development (MCD) [13, 14]. Both mutants are expected to lose MT destabilizing activity, due to a disruption in ATP binding or hydrolysis, thus resulting in a classic form of lissencephaly.

After reaching its peak in the early postnatal weeks, however, the expression of postnatal KIF2A throughout the brain is gradually restricted to specific brain regions, including the hippocampus [15], in which new neurons are generated throughout an

individual's life in established neuronal circuits [16-18]. This postnatal expression pattern suggests that KIF2A might be involved in adult neurogenesis, neuronal migration, and the establishment of refined neuronal circuits in these brain regions, but this role has not yet been confirmed because conventional knockout mice die within one day of birth [9].

In this study, we generated tamoxifen-inducible *Kif2a* conditional knockout (*Kif2a*-cKO) mice to demonstrate the postnatal role of KIF2A in the postnatal brain. We began tamoxifen injections in postnatal week 3 (3w), when the cortical neurons or major cranial nuclei had nearly completed their migration. The 3w-*Kif2a*-cKO mice showed successful neuronal migration, but all mice died by postnatal week 6 and showed signs of hyperactivity, weight loss, and temporal lobe epilepsy (TLE). In the postnatal hippocampus, KIF2A expression was histologically restricted to the dentate mossy fibers (MFs), and the loss of KIF2A induced MF sprouting (MFS) and aberrant recurrent excitatory circuits. In our 3w-*Kif2a*-cKO mouse model, unlike the typical TLE mouse model, the dentate granule cells (DGCs) extended aberrant axons through both the inner and outer molecular layers (IML and OML, respectively). Intriguingly,

primary cultured P3-*Kif2a*-cKO DGCs did not regulate axonal or dendritic length, and consequently, the characteristics of the overextended dendrites changed, resulting in axonal conversion. These results suggested that postnatal KIF2A is a key length regulator of DGC developing neurites and is crucial for establishing postnatal hippocampal wiring.

Results

Weight loss, hyperactivity, and severe epilepsy were exhibited by 3w-*Kif2a*-cKO mice.

To determine the role of KIF2A in the postnatal brain, we generated tamoxifen-induced *Kif2a* conditional knockout mice (*Kif2a*-cKO, Fig. 1A). Before tamoxifen injection, these mice were normal in appearance and did not exhibit any abnormal phenotypes. We injected both wild-type (WT) and *Kif2a*-cKO siblings with tamoxifen for 7 days during the third postnatal week, after the peak expression of KIF2A in the hippocampus (Figs. 1B and 1C). In addition, by the end of the second postnatal week, cortical neurons have almost finished migration and the injection timing was chosen to

83 minimize the neuronal migratory defects in the developing cortex, which are severe in
84 conventional knockout mice [9]. As a result, KIF2A expression was lost in the cKO
85 brain within 1 week of tamoxifen injection (Fig. 1D). These cKO mice were designated
86 3w-*Kif2a*-cKO mice because the tamoxifen injections began at postnatal week 3. As a
87 control for the *Kif2a*-cKO mice, WT siblings were used in all experiments after
88 confirmation that the phenotypes of all siblings except for tamoxifen-injected
89 *Kif2a*-cKO mice were not significantly different.

90 During the postnatal week 4, the 3w-*Kif2a*-cKO mice became smaller than the
91 WT siblings (Fig. 1E) and showed weight loss (Fig. 1F). They also gradually developed
92 hyperactivity (Fig. 1G), twitching, and seizures. An open-field test showed that almost
93 half of the 3w-*Kif2a*-cKO mice experienced an epileptic seizure within 30 min (Fig.
94 1H). Eventually, all 3w-*Kif2a*-cKO mice died by postnatal day 42 (P42), the end of the
95 postnatal week 6 (Fig. 1I). Among them, some 3w-*Kif2a*-cKO mice died immediately
96 after experiencing severe epileptic convulsions, which may have been one of the causes
97 of death. The source data of body weight and activity of 3w-*Kif2a*-cKO mice and all
98 siblings were shown in Figure 1-source data 1.

The epileptic hippocampus was developed in 3w-*Kif2a*-cKO mice.

To determine the focal point of the seizures, we simultaneously recorded electroencephalograms (EEGs) and behavior during postnatal week 5. The electrodes were inserted into the hippocampus and the cortex of WT and 3w-*Kif2a*-cKO siblings. In the hippocampus, 3w-*Kif2a*-cKO mice showed aberrant spikes in the EEG (arrowheads in Fig. 2A) that coincided with twitching in the resting or locomotive state (Figs. 2B and 2C). Moreover, during the epileptic seizure (Figure 2-Video 1), the paroxysmal EEG events were clearly detected in the hippocampus but not in the cortex (Fig. 2D). The source data of those EEG was shown in Figure 2-source data1. These results suggested that the loss of postnatal KIF2A resulted in an epileptic hippocampus in 3w-*Kif2a*-cKO mice.

Supporting evidence for the epileptic hippocampus was provided by three experiments: a histological analysis of the hippocampus of 3w-*Kif2a*-cKO siblings using Bodian's silver staining method, an immunohistological analysis of frozen hippocampal sections of 3w-*Kif2a*-cKO siblings using an anti-glial antibody to detect gliosis, and a physiological analysis of the cultured hippocampal slices from

115 P3-*Kif2a*-cKO siblings collected on P5. The third experiment required P3-*Kif2a*-cKO
116 mice because P4-P6 mice should be used for hippocampal slice cultures [19].

117 The first analysis demonstrated that, although there were no apparent laminar
118 defects (Fig. 2E), the DGCs of 3w-*Kif2a*-cKO mice developed many kinks and
119 defasciculated axons in the CA3 region (Fig. 2F), and were hypertrophic, scattered (Fig.
120 2G) and swollen (Fig. 2H) at the end of the fifth postnatal week, all possible features of
121 hippocampal sclerosis [20], a subsequent complication of hippocampal epilepsy.
122 Moreover, when we began the tamoxifen injections one week later, at postnatal week 4,
123 4w-*Kif2a*-cKO mice clearly showed features of hippocampal sclerosis (Fig. 2S1A) with
124 CA1 loss (Fig. 2S1B), mossy fiber sprouting (Fig. 2S1C), and hypertrophic scattered
125 DGCs (Fig. 2S1D).

126 In the second analysis, frozen sections were stained with an anti-glial fibrillary
127 acidic protein (GFAP) antibody because gliosis is also a sign of an epileptic
128 hippocampus [21-23]. Importantly, the 3w-*Kif2a*-cKO hippocampus contained more
129 GFAP-positive astroglia (Figs. 2S1F and 2S1G, Figure 2-Figure supplement 1-source
130 data 1) than the WT (Fig. 2S1E).

In the third analysis, we attempted to demonstrate the endogenous development of excitatory recurrent circuits in the P3-*Kif2a*-cKO hippocampus. We dissected the hippocampus at postnatal day 5 (P5), sliced it for culturing, and performed an electrophysiological analysis at 10 days *in vitro* (DIV10). We then placed a stimulating electrode into the hilus and a detecting electrode into the granule cell layer (GCL) in the dentate gyrus (Fig. 2S1H) to record the presence of excitatory signals, which would indicate the development of excitatory recurrent circuits in the P3-*Kif2a*-cKO slice. As shown in Figure 2J, an apparent paroxysmal depolarization shift (PDS) was observed in the P3-*Kif2a*-cKO slice (Fig. 2K, Figure 2-source data 2) but not in the WT hippocampus (Fig. 2I), suggesting that the P3-*Kif2*a-cKO hippocampal slices had endogenously developed excitatory recurrent circuits without application of any excitatory drugs, such as picrotoxin. Together, the results suggested that recurrent excitatory circuits are endogenously induced by the loss of KIF2A without extrinsic excitation.

Defects in cell proliferation and cell migration were not significant in the 3w-*Kif2a*-cKO hippocampus.

147 To demonstrate how the loss of postnatal KIF2A contributes to the development of an
148 epileptic hippocampus, we first analyzed neurogenesis and cell migration in the dentate
149 gyrus because abnormally generated or migrated DGCs often affect epileptogenesis,
150 seizure frequency, and seizure severity [24-27]. Two types of thymidine analogs,
151 5-chloro-2'-deoxyuridine (CldU) and 5-iodo-2'-deoxyuridine (IdU), were injected for 7
152 days before and after tamoxifen injection to detect the newly synthesized DNA of
153 replicating cells before and after the loss of KIF2A (Fig. 3A). The brains of injected
154 mice were fixed at P35, and sliced sections were stained with anti-CldU and anti-IdU
155 antibodies. Importantly, the numbers of CldU- and IdU-positive cells were not
156 significantly different between WT and 3w-*Kif2a*-cKO slices (Fig. 3B, Figure 3-source
157 data 1). Then, the vertical distance from the baseline of the GCL (white broken lines in
158 Figs 3C-3F) to the dU-positive cells was calculated. When cells migrated into the GCL
159 or hilus (white and blue arrowheads in Figs. 3E and 3F, respectively), the distance was
160 given a plus (+) or minus (-) value, respectively. Migration histograms show that
161 CldU-positive cells migrated farther than IdU-positive cells, but the difference in the
162 cellular distribution between the WT and 3w-*Kif2a*-cKO mice was not significant (Fig.

3H, compared with 3G, see also Fig. 3I, Figure 3-source data 1).

Aberrant axon terminals of DGCs were widespread throughout the entire molecular layer in 3w-*Kif2a*-cKO mice.

Before further experiments were conducted to elucidate the contribution of KIF2A to the development of an epileptic hippocampus, we analyzed the detailed distribution of KIF2A in the hippocampus by using an anti-KIF2A antibody at P21. As shown in Figure 4A, KIF2A expression was highly localized in the hilus and stratum lucidum of WT mice, where MFs were found (white arrowhead), whereas this effect was absent in 3w-*Kif2a*-cKO mice (Fig. 4B). MFs are the excitatory axons of DGCs [28] and create synapses with their targets, which are pyramidal cells in the CA3, mossy cells in the hilus, and basket cells in the dentate gyrus [29].

In addition, MFs are closely related to TLE as MFS is often observed in the hippocampus of patients and animal models of TLE. Thus, we hypothesized that KIF2A specifically regulates MF elongation and that the loss of KIF2A induces MFS, thus resulting in aberrant excitatory circuits and an epileptic hippocampus. Early reports have also suggested that sprouted MFs contribute to TLE pathogenesis [30].

However, MFS is known to be intimately involved in the deterioration and chronicity of TLE [31]. When TLE occurs, excitation results in MFS, after which these collaterals recurrently elongate into the IML of the dentate gyrus where they form excitatory recurrent circuits. In short, MFS is thought to be a result of TLE.

To verify our hypothesis, we first determined the final destinations of the MFs by using Timm's staining methods. Timm sulfide silver staining is a histochemical technique used to visualize the spatial distribution of MF terminals, which specifically express high levels of Zn^{2+} [32]. For controls, we prepared two different samples: a pilocarpine-induced TLE mouse model [20] as a positive control for hippocampal epilepsy and a carbamazepine (CBZ)-injected 3w-*Kif2a*-cKO mouse model as a negative control in which CBZ blocks voltage-gated sodium channels and suppresses epileptic seizures during continuous use. We aimed to distinguish the effects of KIF2A deficiency from the effects of epileptic excitation on MFS.

In WT mice, Zn-positive axons of DGCs were observed in the hilus and stratum lucidum but not in the stratum oriens (so) or molecular layer (ML) (Fig. 4C). In 3w-*Kif2a*-cKO mice (Fig. 4D), however, the Zn-positive axons were aberrantly

195 elongated in the stratum oriens (yellow arrowheads in Fig. 4F compared with Fig. 4E)
196 and throughout the entire ML (yellow bar in Fig. 4H compared with Fig. 4G).
197 Importantly, the same phenotypes were observed in the CBZ-injected 3w-*Kif2a*-cKO
198 mice (Figs. 4S1B and 4S1D, compared with 4S1A and 4S1C, Figure 4-Figure
199 supplement1-source data 1). Furthermore, the Timm grain intensities in the ML of both
200 3w-*Kif2a*-cKO and CBZ-injected 3w-*Kif2a*-cKO mice were >2-fold higher than those
201 in the respective controls (Figs. 4I and 4S1E, Figure 4-source data 1, Figure 4-Figure
202 supplement1-source data 1). Intriguingly, the signal patterns in the ML of both
203 3w-*Kif2a*-cKO and CBZ-injected 3w-*Kif2a*-cKO mice were different from those in the
204 TLE mouse model in which the signal was restricted to only the IML (Fig. 4J). These
205 results suggested that the aberrant DGC axons of 3w-*Kif2a*-cKO mice extended
206 throughout the ML, regardless of the presence of epileptic seizures.

207 Supporting those results, a different axon marker (neurofilament M, NFM),
208 which specifically detects axons but not dendrites of DGCs in the hippocampus [33, 34],
209 and a DGC-axonal synaptic marker (synaptoporin) both exhibited wider distributions in
210 3w-*Kif2a*-cKO mice than in WT mice (Figs. 4S2B and 4S2E compared with Figs. 4S2A

211 and 4S2D. See also Figs. 4S2C and 4S2F. Figure 4-Figure supplement 2-source data 1
212 and 2).

213 **DGCs showed aberrant morphological changes in axons, cell bodies, and dendritic**
214 **spines in 3w-*Kif2a*-cKO mice.**

215 To investigate the identity of the aberrant DGC axons in the entire ML, we attempted to
216 visualize the morphology of a single DGC in the hippocampus. To this end, *Kif2a*-cKO
217 mice were crossed with *thy1*-YFP transgenic mice (M-line) in which yellow fluorescent
218 protein (YFP) is genetically encoded downstream of the *Thy1* promoter [35] and
219 selectively expressed in a specific neuronal subset. YFP allowed for full visualization of
220 the hippocampal neurons, including their axons, nerve terminals, dendrites, and
221 dendritic spines. The offspring of the cross, *thy1*; YFP; *Kif2a*-cKO mice, were injected
222 with tamoxifen beginning at postnatal week 3, and their tissues were fixed 3 weeks later.
223 We treated 300-μm-thick sliced sections with ScaleView, an optically transparent
224 reagent [36], to clarify the structure of granule cells without decreasing their
225 fluorescence signal.

We focused on three morphological queries (Fig. 5A). The first was whether the origin of aberrant axons in the ML of *Kif2a*-KO mice originated predominately from MFs in the hilus or directly from the cell bodies. The second was whether there were phenotypic differences between immature and mature DGCs. As shown in Figure 5A, after neurogenesis in the subgranular zone (SGZ), DGCs migrate into the GCL and develop a primary axon and an apical dendritic tree [37]. Therefore, at postnatal week 3, immature DGCs in the inner GCL lost KIF2A in the early developmental stage, but DGCs near the ML in the outer GCL lost KIF2A after maturation. The third query related to the effects of KIF2A loss in the dendrites of mature DGCs, because alteration in MT-dynamics often affect spine morphology and function [38-40].

As shown in Figure 5B, WT DGCs in both the inner and outer GCL (orange and red asterisks, respectively) projected a single primary axon into the hilus and extended several apical dendrites into the ML (white arrows). However, 3w-*Kif2a*-cKO mice (Fig. 5C), which were more than 10% of outer mature DGCs, extended an aberrant axon recurrently to the ML (similarly to the cell with a white asterisk), and more than 5% of outer mature DGCs extended aberrant axons directly from the cell body (similarly to the

242 cell with a red asterisk) (Figs. 5C, 5F). In contrast, among inner immature DGCs,
243 almost 30% of the cells had some aberrant protrusions on the cell bodies (orange
244 arrowheads of the cell with orange asterisk in Figs. 5C and 5G). Moreover, there were
245 more ectopic DGCs in the 3w-*Kif2a*-cKO inner ML than in the ML of WT mice (Fig.
246 5H). The source data of those processes were shown in Figure 5-source data 1.

247 In addition, the spine density of the dendrites of outer mature cells was higher in
248 3w-*Kif2a*-cKO mice (Fig. 5E) than in WT mice (Fig. 5D). Morphologically, the number
249 of thin spines, not mushroom or stubby spines, was specifically higher in both the IML
250 and OML of 3w-*Kif2a*-cKO dendrites than in those of WT dendrites (Fig. 5I, Figure
251 5-source data 2). The results suggested that the loss of KIF2A results in more unstable
252 or immature spines.

253 **Cultured *Kif2a*-cKO DGCs showed dendro-axonal conversion from DIV3.**

254 To analyze how DGCs develop and differentiate their axons and dendrites, we prepared
255 a primary culture of dissociated DGCs from P3-*Kif2a*-cKO mice at P5, and
256 characterized their processes with axonal markers (Tau1 or NFM) and dendritic markers
257 (MAP2) at different stages. Before this analysis, we confirmed the DGC characteristics

of the cultured cells and the loss of KIF2A from the DGCs by immunostaining the cells with anti-Prox1 (a DGC marker) and anti-KIF2A antibodies. More than 80% of cultured cells were Prox1-positive (Figs. 6S1A and 6S1B), and almost all cells had lost KIF2A expression (Fig. 6S1C). At DIV1, both WT and P3-*Kif2a*-cKO DGCs generated a short Tau1-dominant axon (Figs. 6B and 6F) and a MAP2-dominant dendrite (Figs. 6C and 6G). At DIV3, however, P3-*Kif2a*-cKO DGCs gradually generated more aberrant axons than they did dendrites. At that time, in WT DGCs, ankyrin G, the marker of the axon hillock, was detected at the neck of one axonal neurite (an arrow in Fig. 6S1E). In the P3-*Kif2a*-cKO DGCs, however, ankyrin G was detected in more than one neurite (arrows in Fig. 6S1H) and the population of DGCs with multiple axonal nurites was significantly larger in P3-*Kif2*-cKO DGCs than in WT DGCS (Fig. 6S1J). Eventually, at DIV5, the WT DGCs developed a single long axon (a white arrowhead in Fig. 6I) and several dendrites (a white arrow in Fig. 6K), whereas P3-*Kif2a*-cKO DGCs developed long, defasciculated, NFM-positive axons (white arrowheads in Fig. 6J) and generated some dendrites with multiple additional axons around their cell bodies (Fig. 6L). A statistical analysis also demonstrated significant neogenesis of aberrant axons in

274 P3-*Kif2a*-cKO DGCs (Fig. 6M green bars, Figure 6-source data 1). These phenotypes
275 were rescued by the KIF2A transfection (Figs. 6S2A-G). The observations suggested
276 that the neogenesis of aberrant axons in P3-*Kif2a*-cKO DGCs could be the result of a
277 cell autonomous process rather than an altered response to the external environment,
278 such as alterations in chemo-attraction/repulsion.

279 Finally, we recorded living DGCs for 24 h at DIV2. In a WT DGC (Figure
280 6-Video 1), both an axon with a single branch and a dendrite are shown to gently
281 elongate and contract. In contrast, P3-*Kif2a*-cKO DGCs did not exhibit length control
282 for axons or dendrites (Figure 6-Video 2). In the video, an axon with a single branch
283 dramatically sprouted and extended multiple branches. Even dendrites actively
284 generated many thin spinous processes. Moreover, some protrusions instantly appeared
285 from the cell body, and then elongated, seemingly contacting one another. After the
286 recording, the DGCs were fixed and stained with anti-Tau1 and anti-MAP2 antibodies
287 (Figs. 6S2H and 6S2I), revealing that the overextended dendrites had axonal
288 (Tau1-positive, arrows in Fig. 6S2I), rather than dendritic characteristics
289 (MAP2-positive, arrowheads in Fig. 6S2I). These results suggested that the loss of

290 postnatal KIF2A might disrupt axon/dendrite determination and induce the development
291 of multiple short axons in the hippocampus, thus resulting in complex networks in the
292 dentate gyrus.

293 **Discussion**

294 In this study, we sought to determine how KIF2A functions in the postnatal
295 hippocampus, especially during the early postnatal weeks when DGCs are establishing a
296 hippocampal network, because hippocampal KIF2A expression is highest in the third
297 postnatal week (Fig. 1B). KIF2A loss at the postnatal week 3 induced weight loss,
298 hyperactivity, and eventually death with an epileptic hippocampus (Figs. 1E-1I, 2D-2K).
299 In the hippocampus at P21, postnatal KIF2A was strongly expressed in dentate MF (Fig.
300 4A), and its loss induced MFS (Fig. 2S1C) and dysfunctional excitatory circuits (Fig.
301 2J), whereas cell proliferation and cell migration were seemingly unaffected (Fig. 3). In
302 the 3w-*Kif2a*-cKO dentate gyrus, younger granule cells developed aberrant protrusions,
303 and older cells developed aberrant apical axons and thinner dendritic spines (Figs.
304 5B-5I). Abnormal morphogenesis of axons and dendrites was also observed in
305 *Kif2a*-cKO cultured DGCs (Fig. 6J). The results suggested that KIF2A plays crucial

306 roles in the development of the precise wiring of neuronal circuits in the hippocampus
307 by controlling the development and maintenance of the neural processes of DGCs
308 (summarized in Fig. 7).

309 **The contribution of KIF2A to the postnatal proliferation and migration of DGCs.**

310 KIF2A was predicted to play an important role in postnatal proliferation or
311 migration, due to its effect as an MT destabilizer [6, 41, 42] and its critical role in
312 proliferation [43, 44] and neuronal migration in the prenatal hippocampus [9]. In this
313 study, however, neither abnormal neurogenesis nor significant migratory defects were
314 detected in 3w-*Kif2a*-cKO mice within 3 weeks after tamoxifen injection (Fig. 3). Thus,
315 from our present results, whether KIF2A is crucial for postnatal neurogenesis and
316 migration is difficult to confirm.

317 However, three weeks may be too short a period to allow for the detection of
318 migratory defects in postnatal neuronal migration as the variation in the migratory
319 distance was greater than the average DGC migration distance. The use of
320 adult-*Kif2a*-cKO such as 8w-*Kif2a*-cKO, which can survive long enough for newborn

DGCs to migrate through the entire DGC layer, may reveal the function of KIF2A in neuronal migration in the future.

The contribution of KIF2A to the development of DGCs.

Previously, KIF2A has been shown to be a key axonal collateral suppressor of prenatal hippocampal pyramidal neurons. The loss of KIF2A, a MT destabilizer, resulted in the activation of MT polymerization at the growth cone and the overextension of neuronal processes [9]. In agreement with its prenatal functions, the expression of postnatal KIF2A was strongly distributed in the MF tract of DGCs in the hippocampus (Fig. 4A), and the loss of KIF2A induced MFS both *in vivo* and *in vitro* (Figs. 2SC, 4F, 6J, and 6S1B), whereas KIF2A transfection rescued the aberrant collaterals (Fig. 6S2D). In addition to KIF2A expression in axons, cultured DGCs expressed KIF2A in the cell bodies and dendrites at DIV1 (Fig. 6A). The loss of KIF2A from DGCs induced the generation of multiple protrusions (Fig. 5C and Figure 6-Video 2) and aberrant axons from the cell bodies both *in vivo* and *in vitro* (Figs. 4H, 5C, and 6L), and resulted in a change in the appearance and characteristics of dendrites (Figs.

336 5E, 5I, and 6L). These effects of KIF2A loss are interesting and may indicate a new
337 function of KIF2A in axon/dendrite determination.

338 The activation of MT polymerization by collapsin response mediator protein
339 (CRMP)-2 is known to be crucial for axon/dendrite determination and morphogenesis in
340 hippocampal pyramidal neurons, [45-47]. Aberrant MT polymerization due to KIF2A
341 loss might abnormally determine the fate of developing neuronal processes as axons. In
342 other words, KIF2A may suppress the elongation of future dendrites by destabilizing
343 MTs during the early stages of neural development.

344 More intriguingly, similar phenotypes of aberrant neurite growth have been
345 associated with knockout mutations of phosphatase and tensin homologs on
346 chromosome 10 (PTEN) in DGCs, which extended multiple long axons both *in vitro*
347 and *in vivo*. The loss of PTEN constitutively activated Akt kinase activity [48] and the
348 mTORC1 pathway [49]. In addition, another phenotype of 3w-*Kif2a*-KO mice
349 resembles the phenotype of *Pten*-KO mice [50]. *Pten*-KO mice showed signs of gliomas,
350 microcephaly, and an epileptic hippocampus [51, 52]. Moreover, PTEN expression in
351 neurons starts postnatally, and *Pten*-KO neurons developed neuronal hypertrophy and a

loss of neuronal polarity. Therefore, the association of KIF2A with a PTEN-related cascade should be further elucidated. We schematically present KIF2A function in DGC development in Figure 7A.

The contribution of postnatal KIF2A loss to hippocampal wiring and epilepsy.

The function of KIF2A in the development of DGCs might affect postnatal hippocampal wiring because DGCs continue to proliferate in the subgranular layer (SGL), migrate through the GCL, and mature, incorporating their new processes into preliminary existing neuronal networks in the hippocampus throughout their life (Fig. 7B, center panel) [16, 18]. In *Kif2a*-cKO mice (Fig. 7B, right panel), inner immature DGCs might develop aberrant protrusions, migrating DGCs might develop aberrant axons, and outer maturing DGCs might incorporate their aberrant processes into the dentate ML and hippocampal circuits. In addition, the spine morphology is altered in dendrites lacking KIF2A. These phenotypes might mainly occur because of a lack of control of MT dynamics and might result in aberrant hippocampal wiring and epileptogenesis.

In addition, some reports have suggested that the integration of aberrantly migrated hilar ectopic granule cells into the dentate gyrus circuitry is responsible for TLE in the pilocarpine mouse model [53] and in TLE patients with early-life status epileptics [54] and febrile seizures [26]. In the IML in 3w-*Kif2A*-cKO mice, ectopic granule cells into the dentate morphologically integrated into the dentate ML, potentially affecting gyrus circuitry and resulting in epileptogenesis in the 3w-*Kif2A*-cKO hippocampus.

However, the influence of TLE on the *Kif2a*-cKO hippocampal phenotypes is still arguable. In ordinary TLE (left panel of Figure 7B), epileptic excitation induced MFS, recurrent extension of sprouted MF into the dentate IML, and aberrant excitatory recurrent circuits in the hippocampus [55-57]. Although we succeeded in decreasing the influence of TLE through anticonvulsant CBZ treatment *in vivo* (Fig. 4S1D), and by reproducing the aberrant neurites in dissociated DGC cultured cells (Figs. 6, 6S1, and 6S2), this approach must still be carefully evaluated when examining the contribution of the loss of KIF2A to the epileptogenesis and phenotypes of 3w-*Kif2a*-cKO mice. For example, regarding the expansion of the aberrant axons throughout the ML in

3w-*Kif2a*-cKO mice, in TLE, many other types of axons in the hippocampus in addition to MFs exhibit sptouting, but those axons are not detected by Timm's stain. In 3w-*Kif2a*-KO mice, MFS may extend into the OML simply because other types of axons did not sprout in our model, thus leaving more “space” for MF sprouting. However, we believe that the “space” might not be greatly different between 3w-*Kif2a*-cKO mice (Fig. 4H) and the 3w-induced TLE animal models (Fig. 4J) because both mice showed TLE beginning at postnatal week 4, and the sprouting of many types of axons, including MFs in the hippocampus, might be induced by TLE in the ML at the same level.

Regarding the regulation of KIF2A function, the phenotypes of tamoxifen-injected *Kif2a*-KO DGCs suggested that KIF2A may possibly contribute to MFS in ordinary TLE. After epileptic fits in the hippocampus, hyper-excitation locally up-regulates brain-derived neurotrophic factor (BDNF) in the target site of the MF projection, the stratum lucidum (SL). The local activity of BDNF in the hilus initiates MFS, thus eventually resulting in hippocampal hyper-excitability [31, 58]. As shown in Figure 4A, KIF2A is highly expressed in the SL, and previous research has shown that

BDNF-derived kinases p21-activated kinase 1 (PAK1) and cyclin-dependent kinase 5 (CDK5) block the function of KIF2A by phosphorylation in cortical neurons [59]; thus, the hyper-excitation-induced local activation of BDNF might potentially block KIF2A function and therefore induce MFS only in the hilus. Detailed analysis of tamoxifen-injected *Kif2a*-KO DGCs would demonstrate the contribution of KIF2A to MFS in ordinary TLE.

The contribution of KIF2A loss to weight loss and hyperactivity.

The 3w-*Kif2a*-cKO mice exhibited weight loss (Fig. 1F) and hyperactivity (Fig. 1G), first becoming hyperactive, then gradually losing interest in food, becoming weak, and eventually dying. The link between these phenotypes and epilepsy remains unclear, but some reports have suggested that these phenotypes are associated with hippocampal dysfunction [60]. Doublecortin (DCX)-KO mice, which exhibit both weight loss and hyperactivity, harbor a neuronal lamination defect in the hippocampus [61]. Tuba1a-KO mice, which are hyperactive, exhibit prominent hippocampal lamination defects [60]. Although 3w-*Kif2a*-cKO mice did not show an apparent hippocampal laminar defect at

P35 (Fig. 2E), ectopic cells in the dentate gyrus or pyramidal cells displaced by sprouted MFs would result in weight loss and hyperactivity.

Moreover, both phenotypes have also often been reported in MCD patients and animal models [62, 63]. Four recently reported *KIF2A*-mutated human pediatric patients with MCD display band heterotopia, posterior predominant pachygyria, a thin corpus callosum, severe congenital microcephaly, and neonatal-onset seizures [14]. Because the patients were young at the time of the report (3 and 5 months old), further research is necessary to confirm the hippocampal phenotypes of *Kif2a*-mutated MCD patients.

Future perspectives

We herein demonstrated that postnatal KIF2A regulates the development of DGCs and the wiring of neuronal circuits in the hippocampus. However, the relevance of the hippocampal phenotypes of *Kif2a*-KO mice to human patients with mutations in *Kif2a* is not certain. In the future, the molecular mechanisms of KIF2A regulation in DGC development and hippocampal wiring should be explored in both KO mice and in human patients. The progress of this line of research will allow for analysis of the pathogenesis of *Kif2a*-related diseases, including schizophrenia [64], juvenile

myoclonic epilepsy [65], mental retardation, ocular defects [66], and MCD [14]. We hope that the collection of data on KIF2A-deficient mice will clarify the pathogenesis of these diseases and lead to a more accurate diagnosis in humans.

Materials and Methods

Key Resources Table

Reagent type (species) or resource	Designation	Source or reference	Identifiers	Additional information
gene (*Mus muscu/us*)	Kif2a	PMID:1447303	MGI:108390	
strain, strain background (*Mus muscu/us*)	C57BU6NJcl, C57BU6JJcl	Clea Japan		
strain, strain background (*Mus muscu/us*)	CreERt(CAG-cre/Esr1)	The Jackson Laboratory	Tg(CAG-cre/Esr1*)5Amc/J(Stock No: 004453)	
strain, strain background (*Mus muscu/us*)	R26R (lacZ expression with the ROSA26 Cre reporter strain)	PMID:9916792		
strain, strain background (*Mus muscu/us*)	Thy1-EGFP line M	The Jackson Laboratory	Tg(Thy1-EGFP)MJrs/J (Stock No: 007788)	
cell line (Mus musculus)	CMTI-1	Merck Millipore	129/Sv-derived ES cell (ESC) line	
antibody	anti-KIF2A (mouse monoclonal)	PMID: 7535303		(1:200)
antibody	anti-KIF2A (rabbit polyclonal)	Thermo Fisher	Thermo Fisher: PA3-16833	(1:1500)
antibody	anti-GFAP(mouse monoclonal)	BO Transduction Laboratory	BO Bioscience: 610565 (Clone 52/GFAP)	(1:200)
antibody	anti-BrdU (mouse monoclonal) for IdU	BO Pharmingen	BO Bioscience: 555627 (Clone 304)	(1:1000)
antibody	anti-BrdU (rat monoclonal) for CldU	Accurate Chemicals	Accurate Chemicals (Clone: BU1/75)	(1:500)
antibody	anti-Tau1 (mouse monoclonal)	Merck Millipore	Merck Millipore: MAB3410 (Clone PC1C6)	(1:1000)
antibody	anti-Neurofilament M (mouse monoclonal)	Sigma	Sigma: N5264 (Clone NN18)	(1:600)
antibody	anti-MAP2 (chicken monoclonal)	Abeam	Abeam: AB5392 (Clone 304)	(1:200)
antibody	anti-Synaptoporin (rabbit polyclonal)	Synapitic Systems	SYSY:102002	(1:300)
antibody	anti-Prox1 (rabbit polyclonal)	Merck Millipore	Merck Millipore: AB5475	(1:10000)
antibody	anti-Ankyrin G (mouse monoclonal)	Thermo Fisher	Thermo Fisher: 338800 (Clone 4G318)	(1:600)
antibody	Alexa 488-, 546-, 555-, 647, (Goat polyclonal)	Molecular Probes		(1:200 -1:500)
recombinant DNA reagent	pEYFP-C1 (vector)	Clontech		
recombinant DNA reagent	YFP-Kif2a (full length)	PMID: 14980225		Progenitors: pEYFP-C1 vector
commercial assay or kit	LA PCR™ Kit	Takara	TaKaRa:RR013A	
chemical compound, drug	Tamoxifen	Sigma	Sigma:T5648	(30 mg/kg body weight/day)

chemical compound, drug	Pilocarpine	Sigma	Sigma: P6503	(290 mg/kg body weight/day},
chemical compound, drug	Scopolamine methyl bromide	Sigma	sigma: 8502	(1 mg/kg body weight/day)
chemical compound, drug	ScaleView	Olympus		
chemical compound, drug	5-iodo-2'-deoxyuridine	Sigma	Sigma: 17125	50 mg/kg
chemical compound, drug	5-chloro-2'-deoxyuridene	Sigma	Sigma: C6891	50 mg/kg
chemical compound, drug	poly-L-lysine	Sigma	Sigma: P-2636	100 mg/ml
chemical compound, drug	Laminin	Invitrogen	Invitrogen: 23017-015	25 µg/ml
software, algorithm	MicroMax 1.3	AccuScan Instrument		
software, algorithm	Clampex 9.2 software	Axon Instruments		
software, algorithm	IMARIS 7.2	Bitplane Zeiss		
software, algorithm	ImageJ 1.51h	NIH		
software, algorithm	SPSS V22	IBM		
machine	MicroMax Monitor	AccuScan Instruments		
machine	Axopatch 1D amplifier	Axon Instruments		

435

436 **Conditional gene targeting of the *Kif2a* gene**

437 A 3loxP-type targeting vector was constructed by using a genomic clone obtained from
438 an EMBL3 genomic library, and genomic fragments were amplified from the
439 129/Sv-derived ES cell (ESC) line CMT1-1 (Chemicon/Millipore, Billerica, MA, USA)
440 by using an LA-PCR kit (Takara, Japan). The CMT1-1 ESCs were transfected with the
441 targeting vector and screened for homologous recombinants using PCR. The 3loxP/+
442 ESCs were electroporated using a pCre-Pac plasmid to remove the selection cassette
443 flanked by loxP sequences. The 2loxP/+ ESCs were injected into blastocysts, and
444 chimeric male mice were obtained and bred with C57BL/6J female mice. Germline
445 transmission was confirmed by PCR using tail DNA samples. *Kif2a*$^{fl/fl}$ mice were
446 produced by an intercross with *Kif2a*$^{fl/+}$ mice. To conditionally delete exons flanked by
447 loxP and driven by the chicken beta-actin promoter/enhancer coupled with the
448 cytomegalovirus (CMV) enhancer (CBA), tamoxifen-inducible Cre transgenic mice
449 (CreERt; CAG-Cre/Esr1; Jax #004453, JAX MICE Laboratories, Bar Harbor, ME,
450 USA) were used. The CBA-CreERt mice were characterized by using lacZ expression
451 with ROSA26 reporter mice (R26R), which have a loxP-flanked STOP sequence

452 followed by the lacZ gene inserted into the gene trap ROSA26 locus (By courtesy of
453 Prof. Soriano [67]). Conventional knockout mice [9] were crossed with CBA-CreERt$^{+/-}$
454 mice to obtain *Kif2a*$^{+/-}$;CBA-CreERt$^{+/-}$ mice. Male *Kif2a*$^{+/-}$; CBA-CreERt$^{+/-}$ mice were
455 mated with female *Kif2a*$^{fl/fl}$ mice to produce offspring that contained the *Kif2a*$^{fl/+}$,
456 *Kif2a*$^{fl/+}$; CBA-CreERt$^{+/-}$, *Kif2a*$^{fl/-}$, and *Kif2a*$^{fl/-}$; CBA-CreERt$^{+/-}$ alleles. Tamoxifen
457 (Sigma, St. Louis, MO, USA, 10 mg/ml) was dissolved in sunflower oil and
458 administered at a dose of 30 mg per kg body weight daily for 7 consecutive days. The
459 *Kif2a* deletion occurred when the tamoxifen-induced Cre recombinase deleted the
460 floxed DNA domain, which was followed by a frameshift during the *Kif2a* RNA
461 translation. Deletion was confirmed by a western blot analysis of the crude extracts of
462 whole brain tissues at P21 by using a monoclonal antibody against the N-terminal
463 region of KIF2A [10]. For control mice, we generally used wild-type mice after
464 ensuring that the *Kif2a*$^{fl/-}$; CBA-CreERt$^{+/-}$ mice and WT mice were not significantly
465 different. The genotypes were determined by PCR of tail DNA or DNA from ES cells
466 with the following primers (see Fig. 1A):
467 F1, 5'-CGCTCATGTGTTTTAAGCTG-3';

R1, 5’- CACCCCACTATAACCCAGCATTCG-3’;

F2, 5’-GCTGCCAGTGACATAGACTAC-3’, and the Neo and Cre

transgenes. The mice were maintained by repeated backcrossing with C57BL/6J mice

(>12 times) in a pathogen-free environment.

TLE model mice

The mice received an intraperitoneal (i.p.) injection of scopolamine methyl bromide

(Sigma, St. Louis, MO, USA, 1 mg/kg) in a sterile saline vehicle (0.9% NaCl, 0.1 ml

total volume) 30 min prior to an injection of pilocarpine to decrease the peripheral

cholinergic effects of pilocarpine. The experimental animals were then i.p. injected with

a single dose of pilocarpine (Sigma, St. Louis, MO, USA, 290 mg/kg), as previously

described [20]. The WT mice were age-matched with treated mice and received a

comparable volume of vehicle.

Behavior tests

WT male mice and 3w-*Kif2a*-cKO (P25 littermates) were used in all behavioral tests in

a blinded manner. The home cage activity tests were conducted using a MicroMax

Monitor (AccuScan Instruments, Columbus, OH, USA) and quantified using a

computer-operated MicroMax 1.3 (AccuScan Instrument, Columbus, OH, USA). The monitor displayed 16 invisible infrared light beams per axis with synchronous filtering, double modulation and digital hysteresis. These beams provide information that describes the movement of an animal in its home cage, thus allowing an animal's behavior to be monitored. Mice that were housed singly in their home cages were placed in the beam boxes for 5 min, and their activity was continually recorded. The measurements used to assess home cage activity included active time. The average amount of active time was analyzed using Student's t-tests. For epilepsy, five mice were isolated in a cage and observed for 30 min. The epileptic mice were genotyped after the observation.

EEG recording

WT and 3w-*Kif2a*-cKO siblings were anesthetized in the postnatal week 4 by using ketamine/xylazine and were surgically implanted with a set of electrodes. Two 0.1-mm diameter silver wires were bonded, including a 1.2-mm-long reference electrode and a 2.0-mm-long working electrode with a hard epoxy resin coat (except for its 0.2-mm-long exposed tip), which served to electrically insulate the probe from the

reference electrode. Dental cement (GC Dental, Tokyo, Japan) was used to fix the electrode set to the skull. The electrode positions in the left hemisphere and the CA1 of the left hippocampus were stereotaxically determined as 1.3/1.3 mm or 2.0/1.8 mm anterior to the bregma and 1.2/1.2 mm or 1.5/1.5 mm lateral to the midline at a depth of 1.3/1.2 mm or 1.5/1.3 mm for the WT or 3w-*Kif2a*-cKO mice, respectively. These differences were due to the differences in the average brain sizes between the two genotypes. EEG recordings were obtained from mice after complete recovery. The electrodes, measurement system, and software were all purchased from Unique Medical (Tokyo, Japan). EEG recordings were obtained from five mice for each genotype. After EEG recordings, we confirmed the electrode position using a histological examination.

Electrophysiology

The patch-clamp recordings of DGCs were obtained at room temperature using an Axopatch 1D amplifier (Axon Instruments, Union City, CA, USA). Patch pipettes (3–5 MΩ) were filled with 122.5 mM Cs gluconate, 17.5 mM CsCl, 10 mM HEPES, 0.2 mM EGTA, 8 mM NaCl, 2 mM Mg-ATP, and 0.3 Na-GTP (pH 7.2, 290–300 mM mOsm). A slice was transferred to a recording chamber and continuously perfused with cold

516 oxygenated ACSF containing 119 mM NaCl, 2.6 mM KCl, 1.3 mM $MgSO_4$, 1 mM
517 NaH_2PO_4, 26 mM $NaHCO_3$, 2.5 mM $CaCl_2$, and 11 mM D-glucose. Single pulse stimuli
518 were delivered by bipolar tungsten electrodes, which were positioned on the hilus far
519 from the recorded cells, to avoid antidromic activation. Absence of antidromic
520 activation contamination was concluded if CNQX-AP-5 completely eliminated any
521 responses to the stimulus. The signals were filtered at 2 kHz, digitized at 10 kHz, and
522 analyzed using Clampex 9.2 software (Axon Instruments, Union City, CA, USA).

523 **Histological analysis**

524 The nervous elements were stained using the standard Bodian method [68, 69]. Briefly,
525 the brains were fixed in FEA (formalin-ethanol-acetic acid: 90 ml of 80% ethanol with
526 5 ml of formaldehyde and 5 ml of glacial acetic acid), dehydrated with ethanol, and
527 embedded in paraffin. The tissue was sectioned at a thickness of 7 μm. The paraffin
528 sections were hydrated in distilled water (DW), and the slides were then incubated in
529 2% Protargol solution for 48 h at 37°C in the dark with 5 g of polished copper shot. The
530 samples were then rinsed 3 times with DW; reduced in 1% hydroquinone for 10 min;
531 rinsed 3 times with DW; immersed in 1% aqueous gold chloride for 10 min; rinsed 3

times with DW; developed in 2% oxalic acid for 20 min; rinsed twice with DW; fixed in 5% sodium thiosulfate for 5 min; rinsed 5 times with DW; dehydrated; and mounted with cover slips.

For brain tissue immunohistochemistry, the mice were perfused with a solution of 4% paraformaldehyde (PFA) and 0.1% glutaraldehyde (GA) in 0.1 M sodium phosphate buffer (PB, pH 7.4). Subsequently, 30-μm-thick frozen slices were rinsed in PBS, fixed for 10 min, permeabilized with 0.1% Triton X-100 in PBS for 10 min, incubated in blocking solution (5% normal goat serum in PBS) for 30 min, and incubated with primary antibodies at 4°C overnight. After the tissues were washed with PBS, secondary antibodies were applied at 4°C overnight. To stain thick sections, 0.1% Triton X-100 was added to the blocking solution. All antibodies were as described in the previous section. To visualize YFP-expressing GCs in mouse brains, the mice were perfused with a fixation solution, and 300-μm-thick sections were immersed in ScaleView (Olympus, Japan), an optically transparent reagent, at 4°C for 24 h. For all experiments, we used littermates for controls and selected slices at comparable positions

547 determined with a brain atlas. The samples were observed under an LSM710 or LSM
548 780 confocal microscope (Zeiss).

549 **Birth-dating analysis**

550 Immunofluorescence detection of two thymidine analogues (CldU and IdU) was
551 performed along with Tuttle's methods [70]. Briefly, 5-iodo-2'-deoxyuridine and
552 5-chloro-2'-deoxyuridene (IdU and CldU; Sigma, St. Louis, MO, USA) were dissolved
553 in saline at 10 mg/ml as stock solution. Proliferating cells in the hippocampus were
554 labeled by sequential intraperitoneal injection at 50 mg/kg for one week before or after
555 tamoxifen injection. All mice were perfused with 4% PFA/PBS, dehydrated with
556 ethanol, and embedded in paraffin. The 7-μm-thick sections were rehydrated with
557 ethanol, washed for 5 min in PBS, and permeabilized with 0.1% Triton-X 100 for 5
558 min; then, antigen retrieval was performed in boiling 0.01 M pH 6.0 sodium citrate
559 buffer for 20 min by using a microwave oven. Slides were immersed in 1.5 N HCL for
560 40 min at RT, washed twice in PBS for 5 min, and immersed in blocking solution (5%
561 goat serum in PBS). Then an anti-IdU antibody diluted in blocking solution was applied
562 and incubated overnight at 4°C. After being agitated in PBS for 20 min in a shaking jar

563 at 37°C, the slices were washed 4 times in PBS, and anti-CldU antibodies diluted in
564 blocking solution were applied and incubated overnight at 4°C. The slides were washed
565 twice for 5 min per wash in PBS, and then, the appropriate secondary antibody solution
566 (1:300) was applied for 2 h at RT. The slices were washed 5 times for 5 min per wash in
567 PBS, and a cover glass was applied with PBS.

568 The distance between the bottom edge of the GCL and the dentate granule cells
569 was measured using IMARIS software (Zeiss).

570 **Timm staining**

571 To visualize zinc and other metals in the hippocampus, 30-μm-thick frozen brain
572 sections were stained using the neo-Timm method with some modifications [32]. The
573 pixel intensities were measured as previously described [31]. Briefly, in an image
574 acquired using a 20× objective, at least five 20 μm × 20 μm cursor points at 20-μm
575 intervals were positioned in each hilus, granular and IML, OML, and subicular area
576 located just outside the hippocampal sulcus. The mean signal intensity (I) within these
577 cursor points was measured at an 8-bit resolution using ImageJ software (NIH, USA).

578 The Timm grain intensity was determined by dividing the values of these subregions by
579 the value of the subiculum (background). The same method was used to measure the
580 NFM intensity. As an internal control, we used the intensity of NFM staining in the
581 hilus, because the intensity in the subicular or other areas in the dentate gyrus was not
582 stable.

583 **Dispersed dentate granule cell cultures**

584 P3-*Kif2a*-cKO and WT mice were euthanized at P5, and their hippocampal dentate gyri
585 were dissected [71]. Each dentate gyrus was trypsinized and gently triturated to isolate
586 cells (3.5×10^4 cells/cm^2), which were placed in a 4-well glass chamber (Nunc, 155411).
587 Chambers were coated with poly-L-lysine overnight at room temperature (Sigma, St.
588 Louis, MO, USA), washed with DW for 2 h twice, and then coated with laminin
589 overnight at 4°C (inquiry) to clearly visualize any morphological differences in the
590 rapid growth of neurites. Dispersed cells were cultured in MEM (Gibco Thermo Fisher,
591 Massachusetts, USA) / Neuro Brew-21 (MACS, Bergisch Gladbach, Germany) at 37°C
592 in a humidified atmosphere containing 5% CO_2. To confirm the characteristics of the

593 cultured neurons, the cells were stained with anti-NFM, anti-MAP2, anti-Prox1, and
594 anti-AnkyrinG antibodies.

595 **Organotypic hippocampal slice cultures**

596 To confirm excitatory recurrent circuits in the tamoxifen-injected *Kif2a*-cKO
597 hippocampus, organotypic hippocampal slice cultures were prepared as previously
598 described [31]. Briefly, P4 mice were deeply anesthetized, and their brains were
599 removed and cut into 300-μm-thick transverse slices using a VR-1200S (Leica
600 Biosystems, Wetzlar, Germany) in a cold oxygenated Gey's balanced salts solution
601 supplemented with 25 mM glucose. Entorhino-hippocampi were dissected and cultured
602 using a membrane interface technique [72]. Briefly, the slices were placed on sterile
603 30-mm-diameter membranes (Millicell-CM; Millipore, Bedford, MA, USA) and
604 transferred to 6-well tissue culture trays. The cultures were fed with 1 ml of 50%
605 minimal essential medium (Invitrogen, Gaithersburg, MD, USA), 25% horse serum
606 (Cell Culture Lab, Cleveland, OH, USA), and 25% HBSS and the cells were maintained
607 in a humidified incubator at 37°C containing 5% CO_2. The medium was changed every
608 3.5 d.

Acknowledgments

We thank Dr. Phil Soriano (Mt. Sinai School of Medicine) for characterizing the CBA-CreERt mice by using ROSA-STOP reporter mice, Mr. Ishidate for assisting with the confocal analysis, Ryuta Koyama (University of Tokyo) for technical suggestions, Prof. Yasuko Noda (Jikei Medical School) for the KIF2A monoclonal antibody and critical discussions, Mr. Yusuke Takahashi for helping statistical analysis, and all members of our laboratory for constructive discussions, technical support, and kind encouragement. The authors thank Ms. Synthia Ishizawa and Nature Research Editing Service for the English language review.

References

1. Hirokawa N, Niwa S, Tanaka Y: **Molecular motors in neurons: transport mechanisms and roles in brain function, development, and disease**. *Neuron* 2010, **68**(4):610-638.

2. Hirokawa N: **Kinesin and dynein superfamily proteins and the mechanism of organelle transport**. *Science* 1998, **279**(5350):519-526.

3. Aizawa H, Sekine Y, Takemura R, Zhang Z, Nangaku M, Hirokawa N:

Kinesin family in murine central nervous system. *J Cell Biol* 1992, **119**(5):1287-1296.

4. Noda Y, Sato-Yoshitake R, Kondo S, Nangaku M, Hirokawa N: **KIF2 is a new microtubule-based anterograde motor that transports membranous organelles distinct from those carried by kinesin heavy chain or KIF3A/B**. *J Cell Biol* 1995, **129**(1):157-167.

5. Miki H, Setou M, Kaneshiro K, Hirokawa N: **All kinesin superfamily protein, KIF, genes in mouse and human**. *Proc Natl Acad Sci U S A* 2001, **98**(13):7004-7011.

6. Desai A, Verma S, Mitchison TJ, Walczak CE: **Kin I kinesins are microtubule-destabilizing enzymes**. *Cell* 1999, **96**(1):69-78.

7. Howard J, Hyman AA: **Microtubule polymerases and depolymerases**. *Curr Opin Cell Biol* 2007, **19**(1):31-35.

8. Moores CA, Milligan RA: **Visualisation of a kinesin-13 motor on microtubule end mimics**. *J Mol Biol* 2008, **377**(3):647-654.

9. Homma N, Takei Y, Tanaka Y, Nakata T, Terada S, Kikkawa M, Noda

641 Y, Hirokawa N: **Kinesin superfamily protein 2A (KIF2A) functions in**
642 **suppression of collateral branch extension**. *Cell* 2003, **114**(2):229-239.
643 10. Noda Y, Niwa S, Homma N, Fukuda H, Imajo-Ohmi S, Hirokawa N:
644 **Phosphatidylinositol 4-phosphate 5-kinase alpha (PIPKα) regulates**
645 **neuronal microtubule depolymerase kinesin, KIF2A and suppresses**
646 **elongation of axon branches**. *Proc Natl Acad Sci U S A* 2012,
647 **109**(5):1725-1730.
648 11. Ogawa T, Hirokawa N: **Microtubule Destabilizer KIF2A Undergoes**
649 **Distinct Site-Specific Phosphorylation Cascades that Differentially**
650 **Affect Neuronal Morphogenesis**. *Cell Rep* 2015, **12**(11):1774-1788.
651 12. Maor-Nof M, Homma N, Raanan C, Nof A, Hirokawa N, Yaron A:
652 **Axonal pruning is actively regulated by the microtubule-destabilizing**
653 **protein kinesin superfamily protein 2A**. *Cell Rep* 2013, **3**(4):971-977.
654 13. Cavallin M, Bijlsma EK, El Morjani A, Moutton S, Peeters EA,
655 Maillard C, Pedespan JM, Guerrot AM, Drouin-Garaud V, Coubes C *et*
656 *al*: **Recurrent KIF2A mutations are responsible for classic**

657 **lissencephaly**. *Neurogenetics* 2017, **18**(2):73-79.

658 14. Poirier K, Lebrun N, Broix L, Tian G, Saillour Y, Boscheron C, Parrini

659 E, Valence S, Pierre BS, Oger M *et al*: **Mutations in TUBG1,**

660 **DYNC1H1, KIF5C and KIF2A cause malformations of cortical**

661 **development and microcephaly**. *Nat Genet* 2013, **45**(6):639-647.

662 15. Lein ES, Hawrylycz MJ, Ao N, Ayres M, Bensinger A, Bernard A, Boe

663 AF, Boguski MS, Brockway KS, Byrnes EJ *et al*: **Genome-wide atlas of**

664 **gene expression in the adult mouse brain**. *Nature* 2007,

665 **445**(7124):168-176.

666 16. Goncalves JT, Schafer ST, Gage FH: **Adult Neurogenesis in the**

667 **Hippocampus: From Stem Cells to Behavior**. *Cell* 2016,

668 **167**(4):897-914.

669 17. Eriksson PS, Perfilieva E, Björk-Eriksson T, Alborn AM, Nordborg C,

670 Peterson DA, Gage FH: **Neurogenesis in the adult human**

671 **hippocampus**. *Nat Med* 1998, **4**(11):1313-1317.

672 18. Kaplan MS, Hinds JW: **Neurogenesis in the adult rat: electron**

673 **microscopic analysis of light radioautographs**. *Science* 1977,
674 **197**(4308):1092-1094.
675 19. Ikegaya Y: **Abnormal targeting of developing hippocampal mossy**
676 **fibers after epileptiform activities via L-type Ca2+ channel activation**
677 **in vitro**. *J Neurosci* 1999, **19**(2):802-812.
678 20. Shibley H, Smith BN: **Pilocarpine-induced status epilepticus results**
679 **in mossy fiber sprouting and spontaneous seizures in C57BL/6 and**
680 **CD-1 mice**. *Epilepsy Res* 2002, **49**(2):109-120.
681 21. Pollen DA, Trachtenberg MC: **Neuroglia: gliosis and focal epilepsy**.
682 *Science* 1970, **167**(3922):1252-1253.
683 22. Gupta RK, Kathuria MK, Pradhan S: **Magnetisation transfer**
684 **magnetic resonance imaging demonstration of perilesional**
685 **gliosis--relation with epilepsy in treated or healed neurocysticercosis**.
686 *Lancet* 1999, **354**(9172):44-45.
687 23. Loewen JL, Barker-Haliski ML, Dahle EJ, White HS, Wilcox KS:
688 **Neuronal Injury, Gliosis, and Glial Proliferation in Two Models of**

689 **Temporal Lobe Epilepsy**. *J Neuropathol Exp Neurol* 2016,
690 **75**(4):366-378.
691 24. Korn MJ, Mandle QJ, Parent JM: **Conditional Disabled-1 Deletion in**
692 **Mice Alters Hippocampal Neurogenesis and Reduces Seizure**
693 **Threshold**. *Front Neurosci* 2016, **10**:63.
694 25. Hester MS, Danzer SC: **Accumulation of abnormal adult-generated**
695 **hippocampal granule cells predicts seizure frequency and severity**. *J*
696 *Neurosci* 2013, **33**(21):8926-8936.
697 26. Koyama R, Tao K, Sasaki T, Ichikawa J, Miyamoto D, Muramatsu R,
698 Matsuki N, Ikegaya Y: **GABAergic excitation after febrile seizures**
699 **induces ectopic granule cells and adult epilepsy**. *Nat Med* 2012,
700 **18**(8):1271-1278.
701 27. Houser CR: **Granule cell dispersion in the dentate gyrus of humans**
702 **with temporal lobe epilepsy**. *Brain Res* 1990, **535**(2):195-204.
703 28. Watson C, Paxinos G, Puelles L: **The mouse nervous system**, 1st ed
704 edn: Elsevier Academic Press; 2012.

29. Amaral DG, Dent JA: **Development of the mossy fibers of the dentate gyrus: I. A light and electron microscopic study of the mossy fibers and their expansions**. *J Comp Neurol* 1981, **195**(1):51-86.

30. Kwak SE, Kim JE, Choi HC, Song HK, Kim YI, Jo SM, Kang TC: **The expression of somatostatin receptors in the hippocampus of pilocarpine-induced rat epilepsy model**. *Neuropeptides* 2008, **42**(5-6):569-583.

31. Koyama R, Yamada MK, Fujisawa S, Katoh-Semba R, Matsuki N, Ikegaya Y: **Brain-derived neurotrophic factor induces hyperexcitable reentrant circuits in the dentate gyrus**. *J Neurosci* 2004, **24**(33):7215-7224.

32. Danscher G, Zimmer J: **An improved Timm sulphide silver method for light and electron microscopic localization of heavy metals in biological tissues**. *Histochemistry* 1978, **55**(1):27-40.

33. Kron MM, Zhang H, Parent JM: **The developmental stage of dentate granule cells dictates their contribution to seizure-induced plasticity**.

J Neurosci 2010, **30**(6):2051-2059.

34. Parent JM, Yu TW, Leibowitz RT, Geschwind DH, Sloviter RS, Lowenstein DH: **Dentate granule cell neurogenesis is increased by seizures and contributes to aberrant network reorganization in the adult rat hippocampus**. *J Neurosci* 1997, **17**(10):3727-3738.

35. Feng G, Mellor RH, Bernstein M, Keller-Peck C, Nguyen QT, Wallace M, Nerbonne JM, Lichtman JW, Sanes JR: **Imaging neuronal subsets in transgenic mice expressing multiple spectral variants of GFP**. *Neuron* 2000, **28**(1):41-51.

36. Hama H, Kurokawa H, Kawano H, Ando R, Shimogori T, Noda H, Fukami K, Sakaue-Sawano A, Miyawaki A: **Scale: a chemical approach for fluorescence imaging and reconstruction of transparent mouse brain**. *Nat Neurosci* 2011, **14**(11):1481-1488.

37. Kempermann G, Jessberger S, Steiner B, Kronenberg G: **Milestones of neuronal development in the adult hippocampus**. *Trends Neurosci* 2004, **27**(8):447-452.

737 38. Jaworski J, Kapitein LC, Gouveia SM, Dortland BR, Wulf PS,
738 Grigoriev I, Camera P, Spangler SA, Di Stefano P, Demmers J *et al*:
739 **Dynamic microtubules regulate dendritic spine morphology and**
740 **synaptic plasticity**. *Neuron* 2009, **61**(1):85-100.
741 39. Hoogenraad CC, Bradke F: **Control of neuronal polarity and**
742 **plasticity--a renaissance for microtubules?** *Trends Cell Biol* 2009,
743 **19**(12):669-676.
744 40. Penazzi L, Bakota L, Brandt R: **Microtubule Dynamics in Neuronal**
745 **Development, Plasticity, and Neurodegeneration**. *Int Rev Cell Mol*
746 *Biol* 2016, **321**:89-169.
747 41. Wordeman L, Mitchison TJ: **Identification and partial**
748 **characterization of mitotic centromere-associated kinesin, a**
749 **kinesin-related protein that associates with centromeres during**
750 **mitosis**. *J Cell Biol* 1995, **128**(1-2):95-104.
751 42. Manning AL, Ganem NJ, Bakhoum SF, Wagenbach M, Wordeman L,
752 Compton DA: **The kinesin-13 proteins Kif2a, Kif2b, and Kif2c/MCAK**

753 **have distinct roles during mitosis in human cells**. *Mol Biol Cell* 2007,
754 **18**(8):2970-2979.
755 43. Ems-McClung SC, Walczak CE: **Kinesin-13s in mitosis: Key players in**
756 **the spatial and temporal organization of spindle microtubules**. *Semin*
757 *Cell Dev Biol* 2010, **21**(3):276-282.
758 44. Chen MH, Liu Y, Wang YL, Liu R, Xu BH, Zhang F, Li FP, Xu L, Lin
759 YH, He SW *et al*: **KIF2A regulates the spindle assembly and the**
760 **metaphase I-anaphase I transition in mouse oocyte**. *Sci Rep* 2016,
761 **6**:39337.
762 45. Bretin S, Reibel S, Charrier E, Maus-Moatti M, Auvergnon N,
763 Thevenoux A, Glowinski J, Rogemond V, Premont J, Honnorat J *et al*:
764 **Differential expression of CRMP1, CRMP2A, CRMP2B, and CRMP5**
765 **in axons or dendrites of distinct neurons in the mouse brain**. *J Comp*
766 *Neurol* 2005, **486**(1):1-17.
767 46. Quach TT, Honnorat J, Kolattukudy PE, Khanna R, Duchemin AM:
768 **CRMPs: critical molecules for neurite morphogenesis and**

769 **neuropsychiatric diseases**. *Mol Psychiatry* 2015, **20**(9):1037-1045.

770 47. Zhang H, Kang E, Wang Y, Yang C, Yu H, Wang Q, Chen Z, Zhang C,

771 Christian KM, Song H *et al*: **Brain-specific Crmp2 deletion leads to**

772 **neuronal development deficits and behavioural impairments in mice**.

773 *Nat Commun* 2016, **7**:11773.

774 48. Gary DS, Mattson MP: **PTEN regulates Akt kinase activity in**

775 **hippocampal neurons and increases their sensitivity to glutamate and**

776 **apoptosis**. *Neuromolecular Med* 2002, **2**(3):261-269.

777 49. Zhou J, Blundell J, Ogawa S, Kwon CH, Zhang W, Sinton C, Powell

778 CM, Parada LF: **Pharmacological inhibition of mTORC1 suppresses**

779 **anatomical, cellular, and behavioral abnormalities in neural-specific**

780 **Pten knock-out mice**. *J Neurosci* 2009, **29**(6):1773-1783.

781 50. Kwon CH, Luikart BW, Powell CM, Zhou J, Matheny SA, Zhang W, Li

782 Y, Baker SJ, Parada LF: **Pten regulates neuronal arborization and**

783 **social interaction in mice**. *Neuron* 2006, **50**(3):377-388.

784 51. Luikart BW, Schnell E, Washburn EK, Bensen AL, Tovar KR,

785 Westbrook GL: **Pten knockdown in vivo increases excitatory drive onto**
786 **dentate granule cells**. *J Neurosci* 2011, **31**(11):4345-4354.
787 52. Althaus AL, Parent JM: **Pten-less dentate granule cells make fits**.
788 *Neuron* 2012, **75**(6):938-940.
789 53. Cameron MC, Zhan RZ, Nadler JV: **Morphologic integration of hilar**
790 **ectopic granule cells into dentate gyrus circuitry in the pilocarpine**
791 **model of temporal lobe epilepsy**. *J Comp Neurol* 2011,
792 **519**(11):2175-2192.
793 54. Muramatsu R, Ikegaya Y, Matsuki N, Koyama R: **Early-life status**
794 **epilepticus induces ectopic granule cells in adult mice dentate gyrus**.
795 *Exp Neurol* 2008, **211**(2):503-510.
796 55. McNamara JO: **Emerging insights into the genesis of epilepsy**. *Nature*
797 1999, **399**(6738 Suppl):A15-22.
798 56. Gu B, Huang YZ, He XP, Joshi RB, Jang W, McNamara JO: **A Peptide**
799 **Uncoupling BDNF Receptor TrkB from Phospholipase Cgamma1**
800 **Prevents Epilepsy Induced by Status Epilepticus**. *Neuron* 2015,

88(3):484-491.

57. Liu G, Gu B, He XP, Joshi RB, Wackerle HD, Rodriguiz RM, Wetsel WC, McNamara JO: **Transient inhibition of TrkB kinase after status epilepticus prevents development of temporal lobe epilepsy**. *Neuron* 2013, **79**(1):31-38.

58. Tamura M, Tamura N, Ikeda T, Koyama R, Ikegaya Y, Matsuki N, Yamada MK: **Influence of brain-derived neurotrophic factor on pathfinding of dentate granule cell axons, the hippocampal mossy fibers**. *Mol Brain* 2009, **2**:2.

59. Ogawa K, Ito Y, Hirokawa N, Shibuya K, Kokubo M, Ogo E, Shibuya H, Saito T, Onishi H, Karasawa K *et al*: **Concurrent radiotherapy and gemcitabine for unresectable pancreatic adenocarcinoma: impact of adjuvant chemotherapy on survival**. *Int J Radiat Oncol Biol Phys* 2012, **83**(2):559-565.

60. Fallet-Bianco C, Loeuillet L, Poirier K, Loget P, Chapon F, Pasquier L, Saillour Y, Beldjord C, Chelly J, Francis F: **Neuropathological**

817 **phenotype of a distinct form of lissencephaly associated with**
818 **mutations in TUBA1A**. *Brain* 2008, **131**(Pt 9):2304-2320.
819 61. Havik B, Degenhardt FA, Johansson S, Fernandes CP, Hinney A,
820 Scherag A, Lybaek H, Djurovic S, Christoforou A, Ersland KM *et al*:
821 **DCLK1 variants are associated across schizophrenia and attention**
822 **deficit/hyperactivity disorder**. *PLoS One* 2012, **7**(4):e35424.
823 62. Stottmann RW, Donlin M, Hafner A, Bernard A, Sinclair DA, Beier
824 DR: **A mutation in Tubb2b, a human polymicrogyria gene, leads to**
825 **lethality and abnormal cortical development in the mouse**. *Hum Mol*
826 *Genet* 2013, **22**(20):4053-4063.
827 63. Stottmann RW, Driver A, Gutierrez A, Skelton MR, Muntifering M,
828 Stepien C, Knudson L, Kofron M, Vorhees CV, Williams MT: **A**
829 **heterozygous mutation in tubulin, beta 2B (Tubb2b) causes cognitive**
830 **deficits and hippocampal disorganization**. *Genes Brain Behav* 2017,
831 **16**(2):250-259.
832 64. Li C, Zheng Y, Qin W, Tao R, Pan Y, Xu Y, Li X, Gu N, Feng G, He L: **A**

833 **family-based association study of kinesin heavy chain member 2 gene**
834 **(KIF2) and schizophrenia**. *Neurosci Lett* 2006, **407**(2):151-155.
835 65. Kapoor A, Ratnapriya R, Kuruttukulam G, Anand A: **A novel genetic**
836 **locus for juvenile myoclonic epilepsy at chromosome 5q12-q14**. *Hum*
837 *Genet* 2007, **121**(6):655-662.
838 66. Jaillard S, Andrieux J, Plessis G, Krepischi AC, Lucas J, David V, Le
839 Brun M, Bertola DR, David A, Belaud-Rotureau MA *et al*: **5q12.1**
840 **deletion: delineation of a phenotype including mental retardation and**
841 **ocular defects**. *Am J Med Genet A* 2011, **155A**(4):725-731.
842 67. Soriano P: **Generalized lacZ expression with the ROSA26 Cre reporter**
843 **strain**. *Nat Genet* 1999, **21**(1):70-71.
844 68. Bodian D: **A new method for staining nerve fibers and nerve endings**
845 **in mounted paraffin sections.** *Anat Res* 1936, **65**:89–97
846 69. Bodian D: **The staining of paraffin sections of nervous tissues with**
847 **activated protargol. The role of fixatives.** *Anat Res* 1937, **69**:153–162
848 70. Tuttle AH, Rankin MM, Teta M, Sartori DJ, Stein GM, Kim GJ,

Virgilio C, Granger A, Zhou D, Long SH *et al*: **Immunofluorescent detection of two thymidine analogues (CldU and IdU) in primary tissue**. *J Vis Exp* 2010(46):2166.

71. Hagihara H, Toyama K, Yamasaki N, Miyakawa T: **Dissection of hippocampal dentate gyrus from adult mouse**. *J Vis Exp* 2009(33):1543.

72. Stoppini L, Buchs PA, Muller D: **A simple method for organotypic cultures of nervous tissue**. *J Neurosci Methods* 1991, **37**(2):173-182.

Figure legends

Figure 1. Hyperactivity, severe epilepsy, and eventual fatality in 3w-*Kif2a*-cKO mice. A-D. The generation of *Kif2a*-cKO mice. A, Schematic diagram of the conditional *Kif2a* targeting strategy. The conventional targeting allele is also shown at the bottom. Tamoxifen-induced Cre recombinase deletes the floxed p, p+1, and p+2 exons. B. Developmental expression of KIF2A in the hippocampus. The expression peaked at P14. C. The timeline for tamoxifen injection. D. The loss of KIF2A. KIF2A expression was lost within one week after the start of the tamoxifen injection. E. 3w-*Kif2a*-cKO mice at P35. The 3w-*Kif2a*-cKO mice developed smaller bodies than the WT mice. F. The weight curves of WT and 3w-*Kif2a*-cKO mice. The cKO mice showed weight loss after the loss of KIF2A (n = 20, results indicate ± SD, *p < 0.01; Welch's t-test). G. Behavioral test. 3w-*Kif2a*-cKO mice showed hyperactivity at postnatal week 5 (n = 10, error bar indicates ± SD, *p < 0.01; Welch's t-test). H. The frequency of epilepsy. The 3w-*Kif2a*-cKO mice showed epileptic convulsions during a 30-min observation during postnatal week 5 (5 mice each from 5 independent experiments, error bar indicates ± SEM, *p < 0.01; Welch's t-test). I. Survival rate of 3w-*Kif2a*-cKO mice (n = 20). These

876 mice began to die starting in postnatal week 5, and all mice died by the end of week 6.

877 Bars: 1 cm in E.

878 **Figure 1-sourse data 1. The raw data of body weight, activity, and survival rate of**

879 **WT and 3w-*Kif2a*-cKO mice.**

880 **Figure 2**. **3w-*Kif2a*-cKO mice develop epileptic hippocampi.**

881 A-D. Electroencephalography (EEG) recordings. A. Representative baseline EEG

882 recordings of WT and 3w-*Kif2a*-cKO hippocampi in postnatal week 6. Some spikes

883 were observed in the cKO brain, even in mice at rest (arrowheads). B-C. Power spectra

884 obtained from a fast Fourier analysis of baseline EEG recordings. Intervals of 4.5 s (for

885 the cKO, the intervals were separated from a paroxysmal EEG recordings by at least 10

886 s) were selected for analysis. Three independent experiments involving 2 mice were

887 performed for each frequency: *$p < 0.01$ (repeated-measures ANOVA). Error bars

888 indicate ± SEMs. D, Representative paroxysmal EEG recordings of the cKO brain at

889 postnatal week 4. The seizure occurred in the hippocampus. The mouse during the ictal

890 phase of the seizure is shown in Figure 2-Video 1. E-H. Development of hippocampal

891 sclerosis in a cKO brain. E. Bodian-stained coronal hippocampus sections at postnatal

week 6. F-G. Magnified images within rectangles “F” (CA3) and “G” (dentate gyrus) in E. Defasciculating fibers (arrowheads in F) and hypertrophic scattered granular cells (arrowheads in G) were observed in the cKO hippocampus. H. Statistical analysis of the cell size. cKO DGCs are larger than the WT cells. The results are shown as the mean ± SD (7 slices each, n = 259 for WT, n=233 for cKO). *p < 0.01 (Welch’s t-test). I-K. An electrophysiological study was used to detect recurrent circuits in hippocampal primary cultures. I-J. Representative electrographs showing data from the WT and cKO hippocampi. The black arrowhead indicates the stimulation time point. The WT slice (I) did not yield a response, and long paroxysmal depolarization shifts (PDSs) were detected in the cKO slice (J). K. Statistical analysis of PDSs. The results are shown as the mean ± SD, n = 45, for five independent experiments involving 3 PDSs from 3 slices each. Abbreviations: ML, molecular layer; GCL, granule cell layer. Bars: 100 μm in E and 10 μm in F, G.

Figure 2-Figure supplement 1. The epileptic hippocampus in tamoxifen-injected *Kif2a*-cKO mice. A-D. The typical features of hippocampal sclerosis in 4w-*Kif2a*-cKO mice at postnatal week 12. The 4w-*Kif2a*-cKO mice clearly showed hippocampal

atrophy (A), including CA1 loss (B), sprouting MFs in CA3 (C), and hypertrophic granule cells (D). E-G. Gliosis in 3w-*Kif2a*-cKO mice. E-F. Representative images of astroglia stained with an anti-GFAP antibody. More astroglia were distributed in the 3w-*Kif2a*-cKO mice. G. Statistical analysis of the GFAP-positive area. The GFAP-positive area of the cKO mice was substantially wider than that of WT mice. The results are shown as the mean ± SD (n = 15, three independent experiments. *$p < 0.01$ (Welch's t-test)). H. Schematic of the patch-clamp recordings of DCGs. A stimulating electrode (Stim) and a recording electrode (Rec) were inserted into the hilus and granule cell layer (GCL). Bars: 100 μm in A and 20 μm in B-F.

Figure 2-Video 1. EEG recordings of 3w-*Kif2a*-cKO mice with hippocampal epilepsy. This recording was obtained at postnatal week 5 in a mouse after an EEG operation at postnatal week 4. The epileptic convulsion continued throughout the video. The EEG wave for this convulsion is shown in Figure 2D.

Figure 2-sourse data 1. EEG recordings of WT and 3w-*Kif2a*-cKO mice.

Figure 2-sourse data 2. The latency and lasted time of PDS occurred in the 3w-*Kif2a*-cKO hippocampal slices.

Figure 3. Defects in cell proliferation and cell migration were not significant in the 3w-*Kif2a*-cKO hippocampus. A. The injection scheme of thymidine analogs and tamoxifen. CldU and IdU were injected during postnatal weeks 2 and 3, respectively. The mice were fixed and double-stained with anti-CldU and anti-IdU antibodies. B. The number of proliferated cells before and after KIF2A loss. The results are the means ± SD. (n = 15, three independent experiments. Student' t-test, CldU p = 0.61, IdU p = 0.52). C-F. Representative images of the immunostained dentate gyrus. E and F are magnified images of C and D. The broken white line indicates the bottom line of the GCL. Note that, in both WT (C and E) and cKO (D and F) mice, CldU-positive cells migrated slightly more than IdU-positive cells, and some aberrant cells migrated backward (blue arrowheads in the hilus) or ectopically (white arrowheads in the OML) from the bottom lines. G-H. Representative graphs of the cell migration ratio. Zero represents the starting line for migrating cells at the bottom of the GCL. The distribution of CldU-positive cells and IdU-positive cells are shown in blue bars and red bars, respectively. I. Statistical analysis of the cell migration ratio. The results are the means ± SEM. The average migration distance of CldU-positive cells (CldU(+)) and

IdU-positive cells (IdU(+)) is not significantly different between WT (G) and cKO (H) cells. CldU (WT; n = 210, cKO; n = 235), and IdU (WT; n = 394, cKO; n = 364), three independent experiments. Welch' t-test, (CldU;p = 0.82, IdU;p = 0.89). Abbreviations: IML, inner molecular layer; OML, outer molecular layer; GCL, granule cell layer; SGZ, sub granular zone. Bars: 20 μm in D and F.

Figure 2-Figure supplement 1-source data 1. GFAP-positive area in WT and 3w-*Kif2a*-cKO dentate gyrus at P35.

Figure 3-source data 1. The migrating distance, direction, and expression of birth-dating marker of WT and 3w-*Kif2a*-cKO DGCs at P35.

Figure 4. Zn-positive axon terminals of DGCs are aberrant and widespread throughout the whole ML in the 3w-*Kif2a*-cKO mice.

A-B. The expression of postnatal KIF2A in the hippocampus at P21. Note that KIF2A is highly expressed in the dentate hilus (Hil) and stratum lucidum (SL) (A) where DGCs extend their axons, termed MFs. The loss of KIF2A was observed in the cKO hippocampus (B). C–H. Representative images showing Timm staining of the hippocampus at P35. E–H are magnified images indicated by the red rectangles in C-D.

956 Coronal cryosections in the hippocampus were processed for Timm histochemistry. An
957 abnormally high dark brown density of the reaction product was observed in the SO
958 (yellow arrowheads in F) and the entire dentate ML (a yellow bar in H) in the cKO mice
959 compared to that in the WT mice. I. Statistical analysis of Timm grain intensities.
960 Intensities in OML and IML were significantly higher in the cKO mice than in the WT
961 mice. The results are shown as the mean ± SEMs (5 slices each, n = 6). *$p < 0.01$;
962 Welch's t-test. J. Positive control for the pilocarpine-induced TLE mouse model. Note
963 that Timm reaction products are observed only in the IML (a yellow bar). Broken lines
964 indicate the hippocampal sulcus (G), which forms a boundary between the ML and the
965 SBI. Abbreviations; SL, stratum lucidum; SO, stratum oriens; SBI, subiculum; DGC,
966 dentate granule cells; MF, mossy fiber; IML/OML, inner/outer molecular layer; GCL,
967 granule cell layer. Bars: 400 μm in D and 100 μm in F, H, and I. See the figure
968 supplement as well.

969 **Figure4-source data 1. Timm grain intensity in WT and 3w-*Kif2a*-cKO dentate**
970 **gyrus at P35.**

Figure 4-Figure supplement 1. The Zn-positive axons of DGCs abnormally extended into the SO and the entire ML in the CBZ-injected 3w-*Kif2a*-cKO mice.

A–D. Representative images showing Timm staining of the hippocampus at P35. C and D are magnified images of the areas indicated by the red rectangles in A and B. Coronal cryosections in the hippocampus were processed for Timm histochemistry. Similar to the results for the untreated cKO hippocampus, a large amount of dark brown reaction product was present in the SO (yellow arrowheads in B) and the entire ML (arrowheads in D) in CBZ-injected cKO mice. Broken lines indicate the hippocampal sulcus (C). E. Statistical analysis of Timm grain intensities. The OML and IML intensities were significantly higher in the CBZ-injected cKO mice than in the WT mice. The results are shown as the mean ± SEMs (5 slices each, n = 8). *$p < 0.01$; Welch's t-test.

Abbreviations; SO, stratum oriens; SBI, subiculum; IML/OML, inner/outer molecular layer; GCL, granule cell layer. Bars: 400 μm in B, 100 μm in D.

Figure 4-Figure supplement 1-source data 1. Timm grain intensity in CBZ-injected-WT and CBZ-injected-3w-*Kif2a*-cKO dentate gyrus at P35.

Figure 4-Figure supplement 2. More DGC axons were present throughout the ML of the 3w-*Kif2a*-cKO mice than in that of WT mice. A-B. Representative images of cryosections immunostained with anti-NFM and anti-MAP2 at P35. Images are 1-μm-thick confocal optical sections (OS). Compared with WT (A), 3w-*Kif2a*-cKO mice had more NFM-positive axons in the ML (B). C. Statistical analysis of the NFM staining intensity. The results are shown as the mean ± SEMs (5 slices each, n = 5). *p < 0.01; Welch's t-test. D-E. Representative images of the ML immunostained with a marker of DGC axons, anti-synaptoporin, at P35. The images are 1-μm-thick confocal OSs. Note the lack of obvious synaptoporin staining in the WT OML (D) but the presence of aberrant synaptoporin staining in the cKO OML (E). F. Statistical analysis of intensity, as quantified in 2-μm-thick OSs in the ML. The procedures were similar to the procedures used for the Timm grain intensity analysis. All statistical results are shown as the mean ± SEMs for 5 slices each; n = 6, *p < 0.01, **p < 0.05; Welch t-test. Abbreviations; IML/OML, inner/outer molecular layer; GCL, granule cell layer. Bars: 100 μm in B and E.

Figure 4-Figure supplement 2-source data 1. Intensity of NFM-staining in WT and 3w-*Kif2a*-cKO dentate gyrus at P35.

Figure 4-Figure supplement 2-source data 2. Intensity of Synaptoporin-staining in WT and 3w-*Kif2a*-cKO dentate gyrus at P35.

Figure 5. DGCs developed aberrant morphological changes in axons, cell bodies, and dendritic spines in 3w-*Kif2a*-cKO mice.

A. Schematics of unsolved questions in developing DGCs in the *Kif2a*-cKO dentate granule layer (DGL). In the postnatal hippocampus (left panel), DGCs continuously proliferated in the SGL, migrated through the GCL, and then incorporated newly developed neurites into the existing hippocampal wiring. In 3w-*Kif2a*-cKO mice (right panel), the origin of overextended axons (Q1) and the difference in the immature and mature DGC phenotypes (Q2) and dendritic morphology (Q3) needs to be investigated.

B-C. Representative images of GFP-expressing DGCs. Z-stacked images of 300-μm-thick slices were acquired and reconstructed in 3D. In the outer area of the DGL, some mature cKO DGCs (a red asterisk in C) were aberrantly located in the IML, and developed an aberrant apical axon (red arrowheads in C), whereas WT DGCs (a red

asterisk in B) extended single axons (white arrows in B) and thick dendrites (white arrowheads in B). In the middle area, some cKO DGCs (a white asterisk in C) developed recurrent axons (white arrowheads in C), whereas WT DGCs (white asterisks in B) did not. In the inner area, some cKO immature DGCs (an orange asterisk in C) developed multiple aberrant protrusions (orange arrowheads in C), whereas WT DGCs only showed a slight development of protrusions. D-E. Representative images of the dendrites of matured DGCs. Z-stack images of dendrites in the IML and OML were acquired and reconstructed in 3D. Note that the spines of cKO mice appeared thinner (E) than those of the WT mice (D). F-H, Statistical analysis of inner immature DGCs with apical axons (F) and cells with protrusions (G) and the number of ectopic DGCs (H). Cell bodies were counted in 50-μm-thick OSs (5 slices each from 5 mice; results indicate the mean ± SDs *$p < 0.01$, Welch's t-test). I. Statistical analysis of spine density. The total spine densities were higher in both the OML and IML of cKO mice than in those of WT mice. Morphologically, the density of thin spines was especially increased in cKO mice compared to that in WT mice. The results indicate the mean ± SDs, $n = 5$, *$p < 0.05$, Welch's t-test. Bars: 20 μm in C, and 1 μm in D and E.

Figure 5-source data 1. The population of the cells with apical axons in the outer ML, the cells with protrusion in the inner ML, and the ectopic cells in inner ML in WT and 3w-*Kif2a*-cKO dentate gyrus at P35.

Figure 5-source data 2. The spine morphology of dendrites in IML and OML of WT and 3w-*Kif2a*-cKO dentate gyrus at P35.

Figure 6. Both axons and dendrites were aberrantly developed in cultured P3-*Kif2a*-cKO DGCs. A-L, Representative images of dissociated cultured DGCs immunostained with an axon marker (NFM or Tau1) and a dendrite marker (MAP2) at DIV1 (A-H) and DIV5 (I-L). At DIV1, both WT DGCs (A-D) and cKO DGCs (E-H) extended an axonal process (a arrowhead) and a dendritic process (an arrow). KIF2A was expressed in both processes (A compared with E). At DIV5, WT DGCs developed a single primary axon (an arrowhead in I) and several dendrites (an arrow in K), whereas cKO DGCs developed aberrant collateral branches from a primary axon (arrowheads in J) and multiple aberrant axons originating from their cell bodies (a white arrow and yellow arrowheads in L) in addition to some dendrites. K and L are magnified images of the regions indicated by the dashed squares in I-J. M, DGC neuronal processes at DIV5.

1049 The numbers of processes, not including primary axons, were counted. A

1050 MAP2-positive dendrite (D), MAP2A- and NFM- or Tau1-positive processes (D/A) and

1051 NFM- or Tau1- positive aberrant axons (A) are shown. The results are shown as the

1052 mean ± SEMs for 20 cells each; n = 120. Error bars pointing downward indicate the

1053 SEMs for each type of neurite. The error bars pointing up indicate the SEMs for the

1054 total number of processes (*$p < 0.01$, Welch's t-test). Bars: 100 μm in J, 50 μm in D, H,

1055 and L.

1056 **Figure 6-source data 1. The character of neuronal processes from a cell body of**

1057 **WT and P3-*Kif2a*-cKO DGCs.**

1058 **Figure 6-Video 1. Time lapse recordings of cultured WT DGC.** This recording was

1059 obtained at the end of DIV2 for 8 hours. The DGC controls the length of an axon and a

1060 dendrite. No protrusions from the cell body. An immunostained image of the recorded

1061 cell is shown in Figure 6S1H.

1062 **Figure 6-Video 2. Time lapse recordings of cultured P3-*Kif2a*-cKO DGC.** This

1063 recording was obtained at the end of DIV2 for 8 hours. The DGC is rapidly elongating

and branching an axon and dendrites, in addition to some aberrant protrusions from the cell body. An immunostained image of the recorded cell is shown in Figure 6S1I.

Figure 6-Figure supplement 1. The loss of KIF2A induced MF sprouting in dissociated cultured DGCs.

A-C. Characterization of dissociated cultured granule cells and confirmation of their loss of KIF2A. A-B. Representative images of cultured DGCs. Granule cells from the hippocampal dentate gyri of the WT (A) and *Kif2a*-cKO (B) mice were cultured for 4 days (DIV4) and then the cells were fixed and stained with an anti-Prox1 antibody. C. KIF2A deletion in cultured DGCs. KIF2A expression was analyzed using western blot analysis in extracts from the WT and *Kif2a*-cKO cultured cells obtained on DIV4. D-I. Representative images of ankyrin G-positive neurites in WT (D-F) and P3-*Kif2a*-cKO (G-I) cultured DGCs. At an early stage of DGC development, all neurites are MAP2-positive around the cell body (D and G, see also Fig. 6A). Among those developing neurites, there were more neurites with ankyrin G at the neck in cKO DGCs (arrowheads in H) than in WT DGCs (arrowheads in E). Statistical analysis of the population of DGCs with the number of ankyrin G-positive neurites/cell is shown in J.

1080 The results are shown as the mean ± SDs for approximately 60 cells each; n = 4. (*p <

1081 0.001, Welch's t-test). Bars: 50 μm in B, F and I.

1082 **Figure 6-Figure supplement 1-source data 1. The number of Ankyrin G-positive**

1083 **processes from a cell body of of WT and P3-*Kif2a*-cKO DGCs at DIV3.**

1084 **Figure 6-Figure supplement 2. Transfection of KIF2A rescued MF sprouting in**

1085 **dissociated cultured DGCs.** A-G. The rescue experiment. A-D. Representative images

1086 of single cultured DGCs. DGCs were transfected with YFP or YFP-KIF2A at DIV3 and

1087 then observed at DIV4. Compared with the WT DGCs (A), cKO DGCs developed many

1088 collaterals (B, C). The phenotype was rescued by expressing YFP-KIF2A (D). E-G,

1089 Statistical analysis of the length of primary axons (E), the number of collaterals per

1090 100-μm-long primary axon (F) and the total lengths of the collaterals (G). Note that the

1091 cKO DGCs developed significantly more and longer collaterals than did the WT DGCs.

1092 The results are shown as the mean ± SEM from three independent experiments

1093 including n = 30 cells each. *p = 0.01, One-way ANOVA. H-I. Characterization of

1094 recorded neuronal processes. After recording, the DGCs were fixed and immunostained

1095 with anti-Tau1 and anti-MAP2 antibodies. Dendritic processes that were actively

overextended in the cKO DGC video are Tau1-positive (arrows in I), whereas the WT DGC had a single Tau1-positive axon and MAP2-positive dendrites (an arrow and an arrowhead in H).

Figure 7 Schematic of the function of KIF2A in the postnatal hippocampus. A. KIF2A function in DGC development. At the early stages of development, both WT and cKO DGCs normally make axonal and dendritic processes. However, whereas WT DGCs regulate the length of dendritic processes and extend a primary axon, *Kif2a*-cKO DGCs overextend and sprout both axon and dendrites, eventually developing many sprouted axonal processes. B. KIF2A function in postnatal hippocampal wiring. In WT mice (center panel), KIF2A is highly expressed in MFs (yellow area) and actively suppresses both aberrant MFS and the elaboration of aberrant processes. The excitation of DGCs is unidirectionally transmitted along a MF (blue arrow). When the suppression is released by the loss of KIF2A (right panel), DGCs might start sprouting MFs, thus generating aberrant apical axons, and altering the dendritic features. The aberrant processes are extended into the entire ML and make reflective excitatory circuits. The excitation of DGCs is multidirectionally transmitted, and DGCs are recurrently excited

(orange arrows). The repetitive excitation enhances MFS and then eventually causes TLE. In TLE mice (left panel), repetitive excitation induces MFS, but the distribution of aberrant axon terminals is limited to the IML.

Figure 1

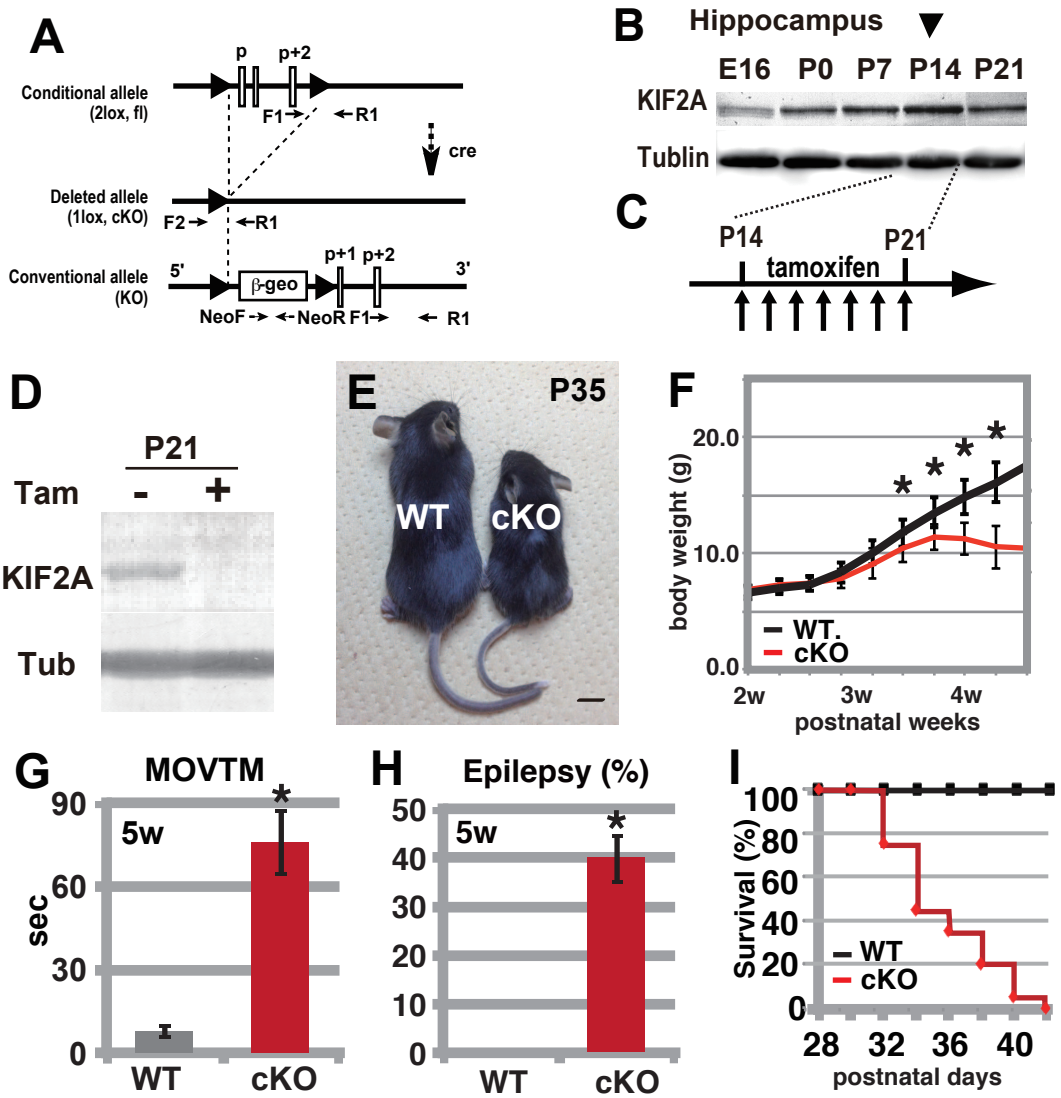
A
p
p+2
Conditional allele
(2lox, fl)
F1
R1
cre
Deleted allele
(1lox, cKO)
F2
R1
Conventional allele
(KO)
5'
β-geo
p+1 p+2
3'
NeoF
NeoR F1
R1
B
Hippocampus
E16 P0 P7 P14 P21
KIF2A
Tublin
C
P14
P21
tamoxifen
D
P21
Tam
-
+
KIF2A
Tub
E
P35
WT
cKO
F
20.0
10.0
0.0
body weight (g)
WT.
cKO
2w
3w
4w
postnatal weeks
G
MOVTM
5w
90
60
30
0
sec
WT
cKO
H
Epilepsy (%)
5w
50
40
30
20
10
0
WT
cKO
I
100
80
60
40
20
0
Survival (%)
WT
cKO
28
32
36
40
postnatal days

Figure 2

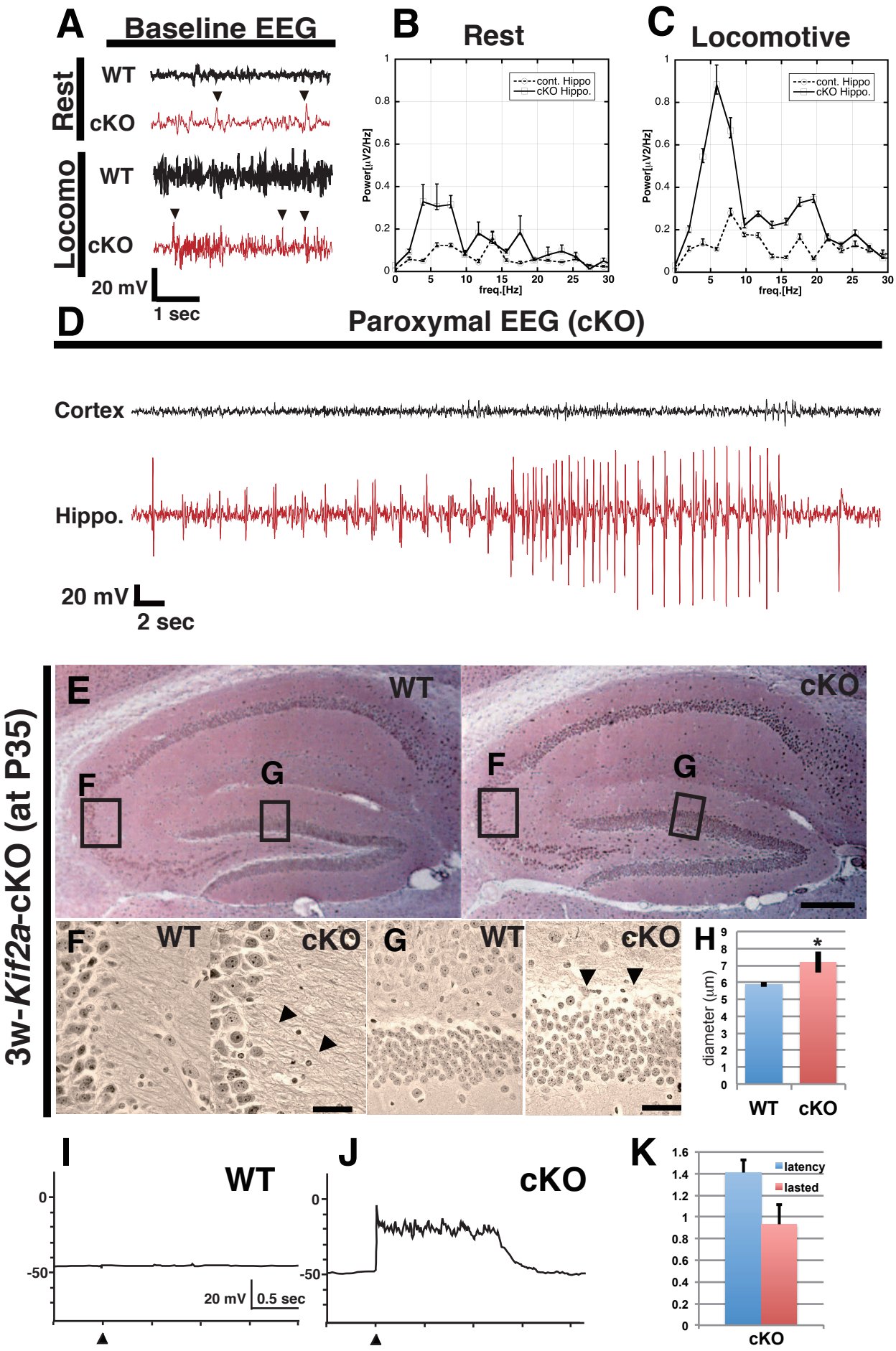
A
Baseline EEG
Rest
WT
cKO
Locomo
WT
cKO
20 mV
1 sec
B
Rest
cont. Hippo
cKO Hippo.
Power[μV2/Hz]
freq.[Hz]
C
Locomotive
cont. Hippo
cKO Hippo.
Power[μV2/Hz]
freq.[Hz]
D
Paroxymal EEG (cKO)
Cortex
Hippo.
20 mV
2 sec
3w-Kif2a-cKO (at P35)
E
WT
cKO
F
G
F
WT
cKO
G
WT
cKO
H
diameter (μm)
WT
cKO
I
WT
0
-50
20 mV
0.5 sec
J
cKO
0
-50
K
latency
lasted
cKO

Figure 2-figure supplement 1

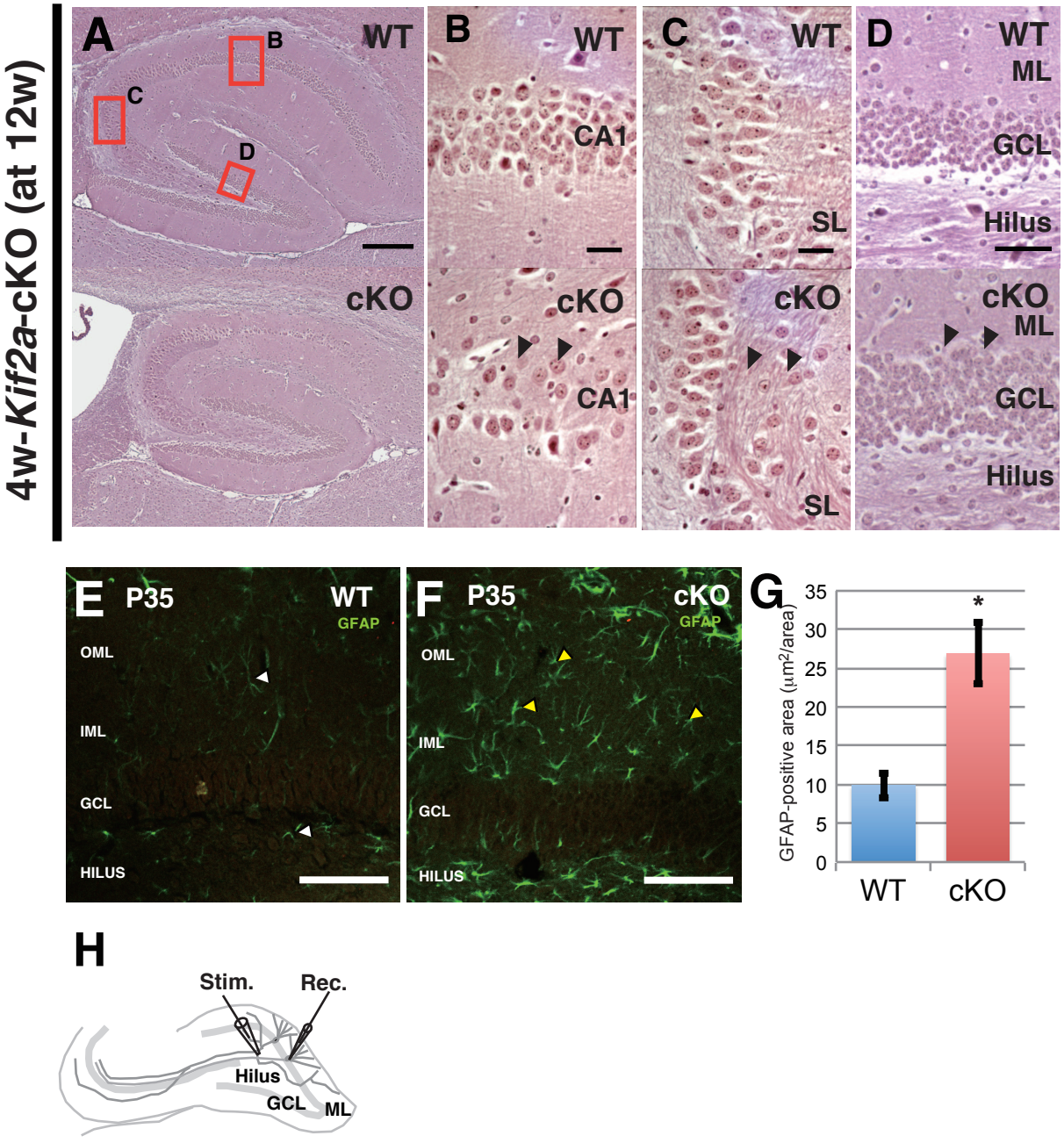

Figure 3

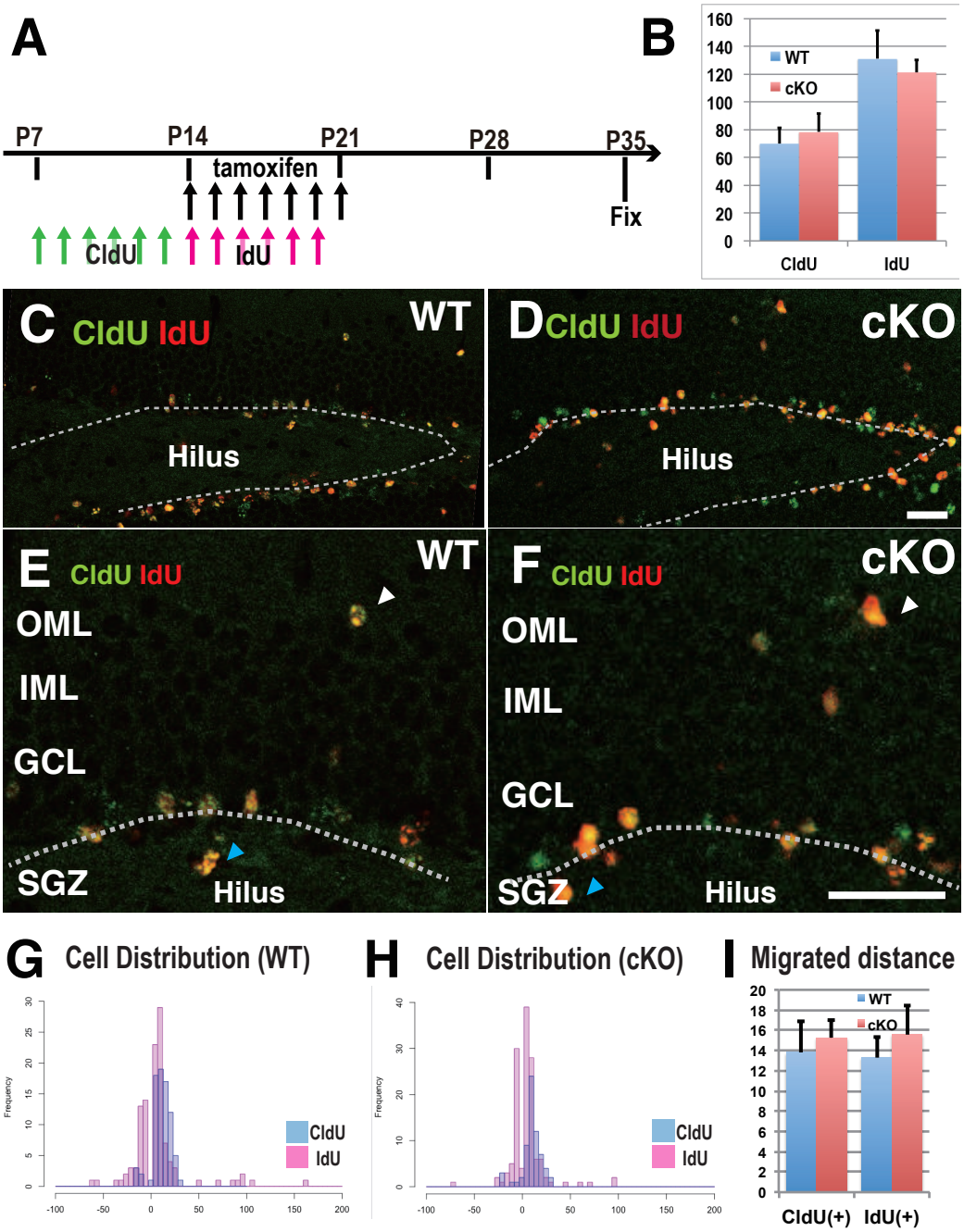
A
P7
P14
P21
P28
P35
tamoxifen
Fix
CldU
IdU
B
WT
cKO
CldU
IdU
C CldU IdU
WT
Hilus
D CldU IdU
cKO
Hilus
E CldU IdU
WT
OML
IML
GCL
SGZ
Hilus
F CldU IdU
cKO
OML
IML
GCL
SGZ
Hilus
G Cell Distribution (WT)
Frequency
CldU
IdU
H Cell Distribution (cKO)
Frequency
CldU
IdU
I Migrated distance
WT
cKO
CldU(+)
IdU(+)

Figure 4

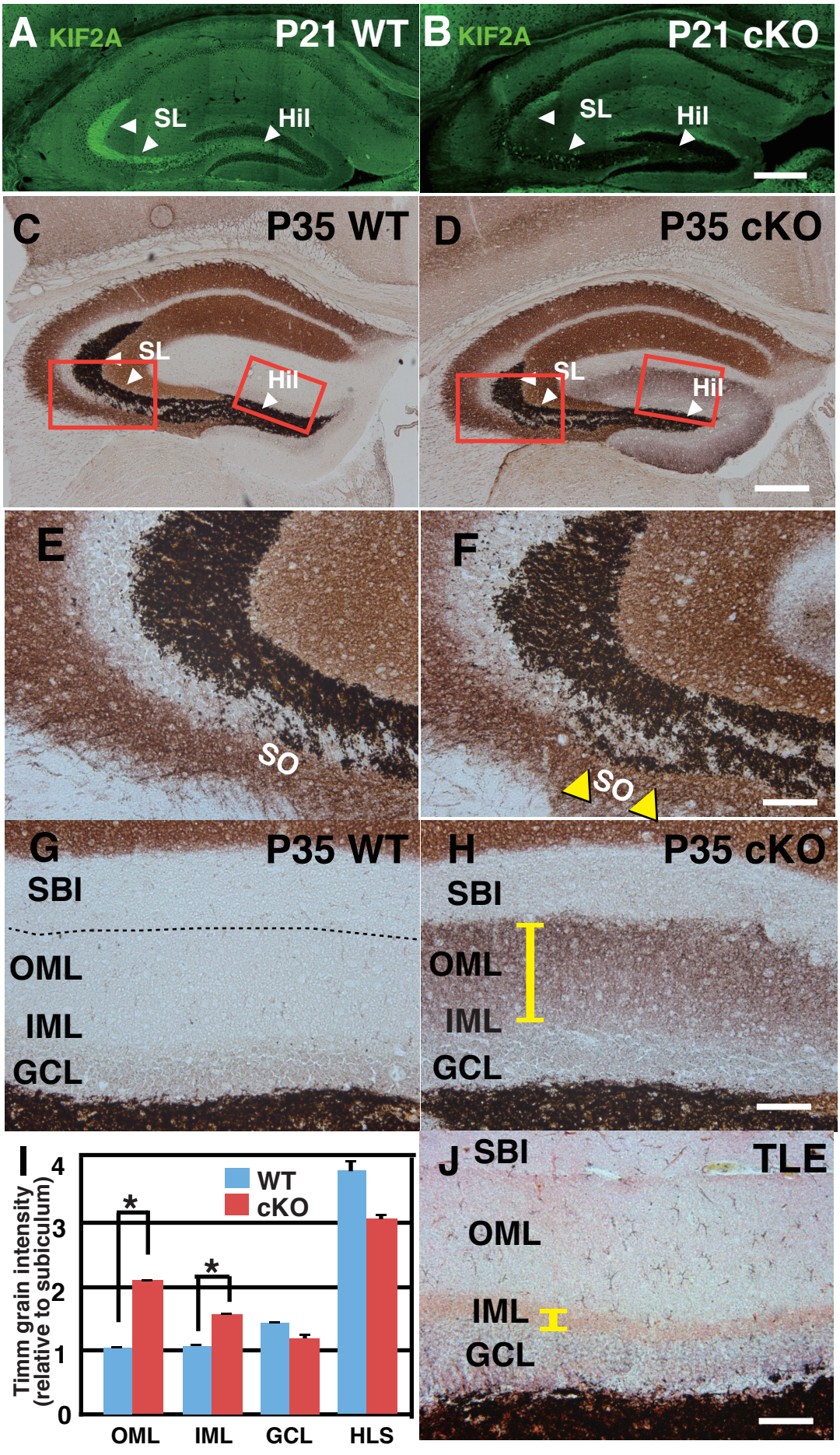
A KIF2A
P21 WT
SL
Hil
B KIF2A
P21 cKO
SL
Hil
C
P35 WT
SL
Hil
D
P35 cKO
SL
Hil
E
SO
F
SO
G
P35 WT
SBI
OML
IML
GCL
H
P35 cKO
SBI
OML
IML
GCL
I
Timm grain intensity (relative to subiculum)
0
1
2
3
4
WT
cKO
*
*
OML
IML
GCL
HLS
J
SBI
TLE
OML
IML
GCL

Figure 4-figure supplement 1

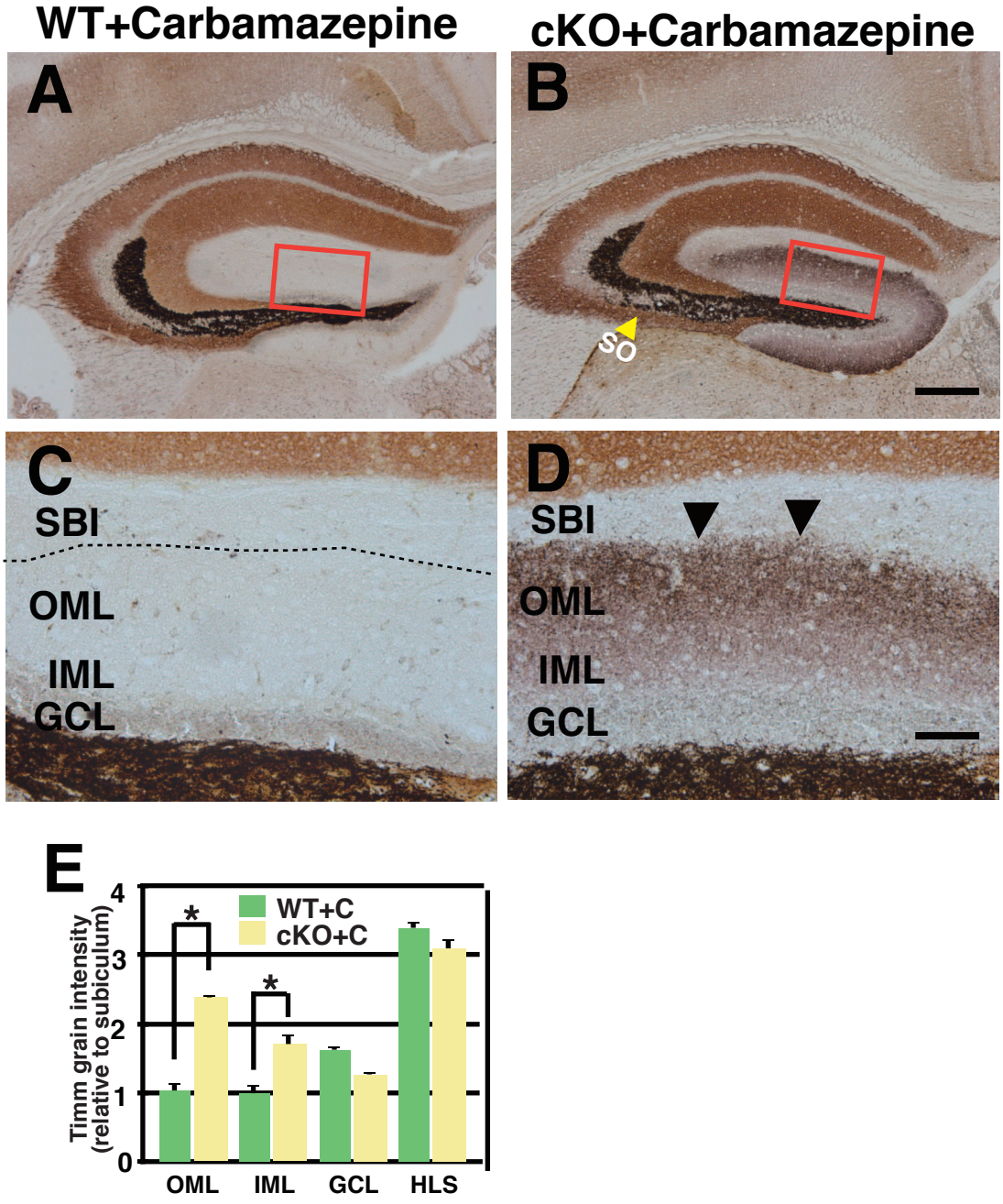

Figure 4-figure supplement 2

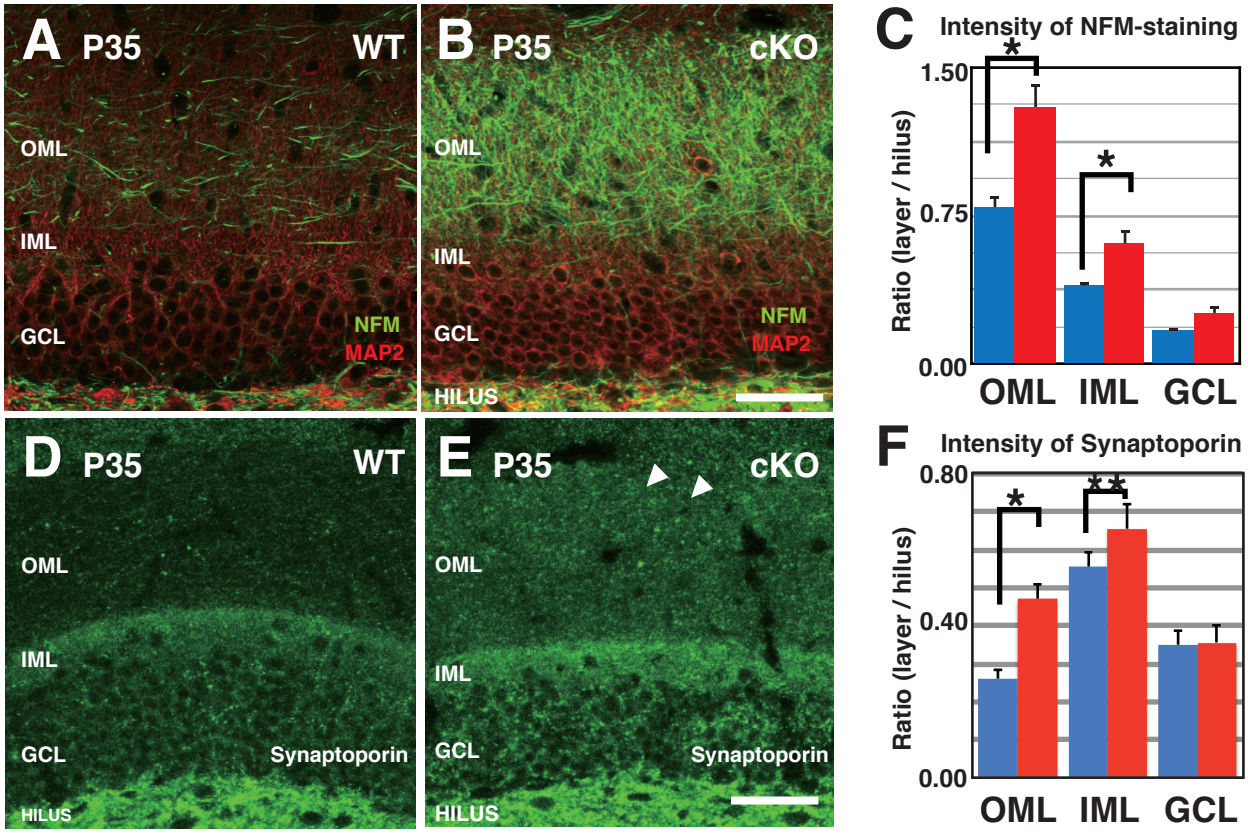

Figure 5

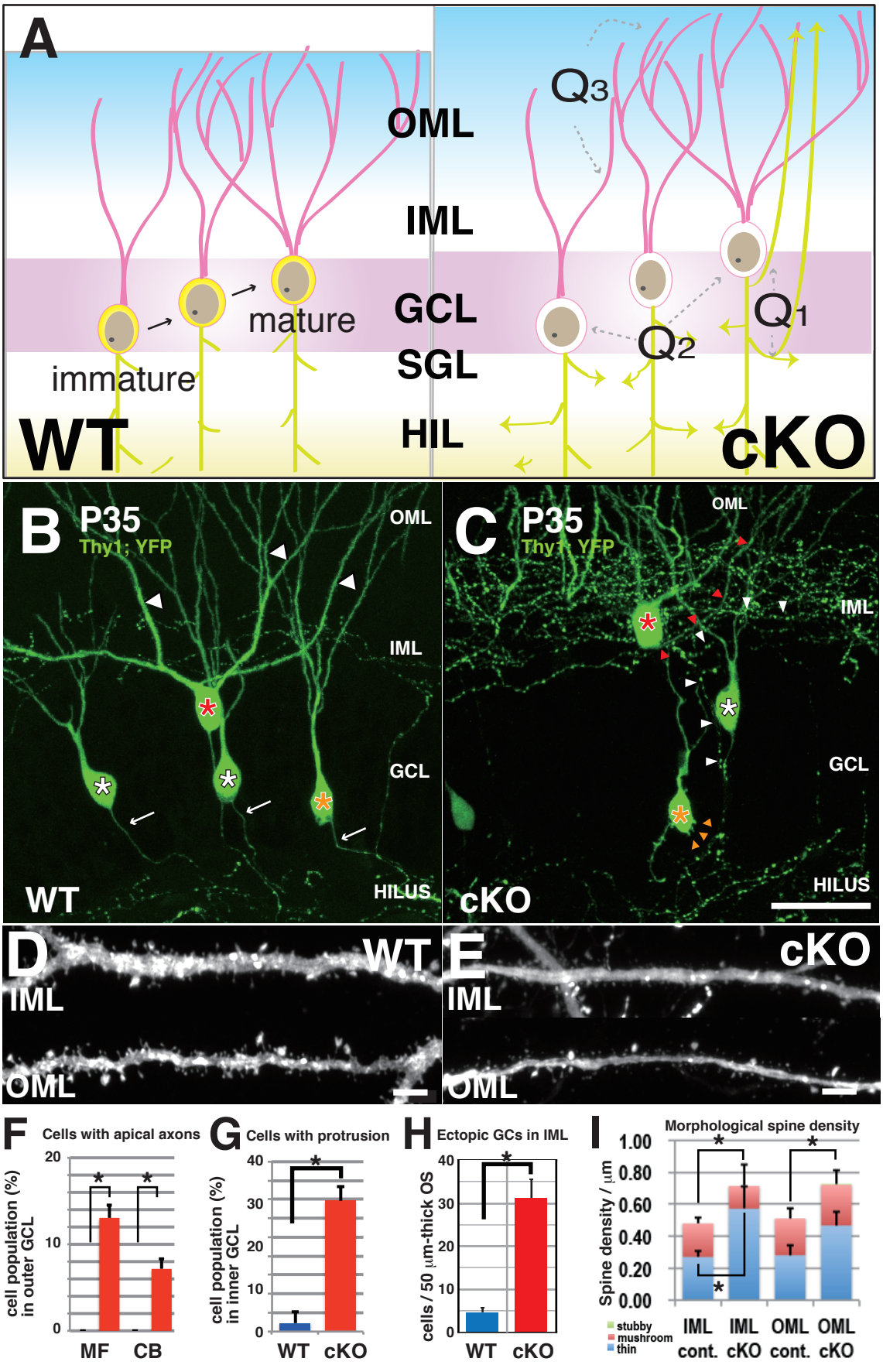
A
OML
IML
GCL
SGL
HIL
mature
immature
WT
Q3
Q2
Q1
cKO
B
P35
Thy1; YFP
OML
IML
GCL
HILUS
WT
C
P35
Thy1; YFP
OML
IML
GCL
HILUS
cKO
D
WT
IML
OML
E
cKO
IML
OML
F
Cells with apical axons
cell population (%) in outer GCL
20
10
0
MF
CB
G
Cells with protrusion
cell population (%) in inner GCL
40
30
20
10
0
WT
cKO
H
Ectopic GCs in IML
cells / 50 μm-thick OS
40
30
20
10
0
WT
cKO
I
Morphological spine density
Spine density / μm
1.00
0.80
0.60
0.40
0.20
0.00
stubby
mushroom
thin
IML cont.
IML cKO
OML cont.
OML cKO

Figure 6

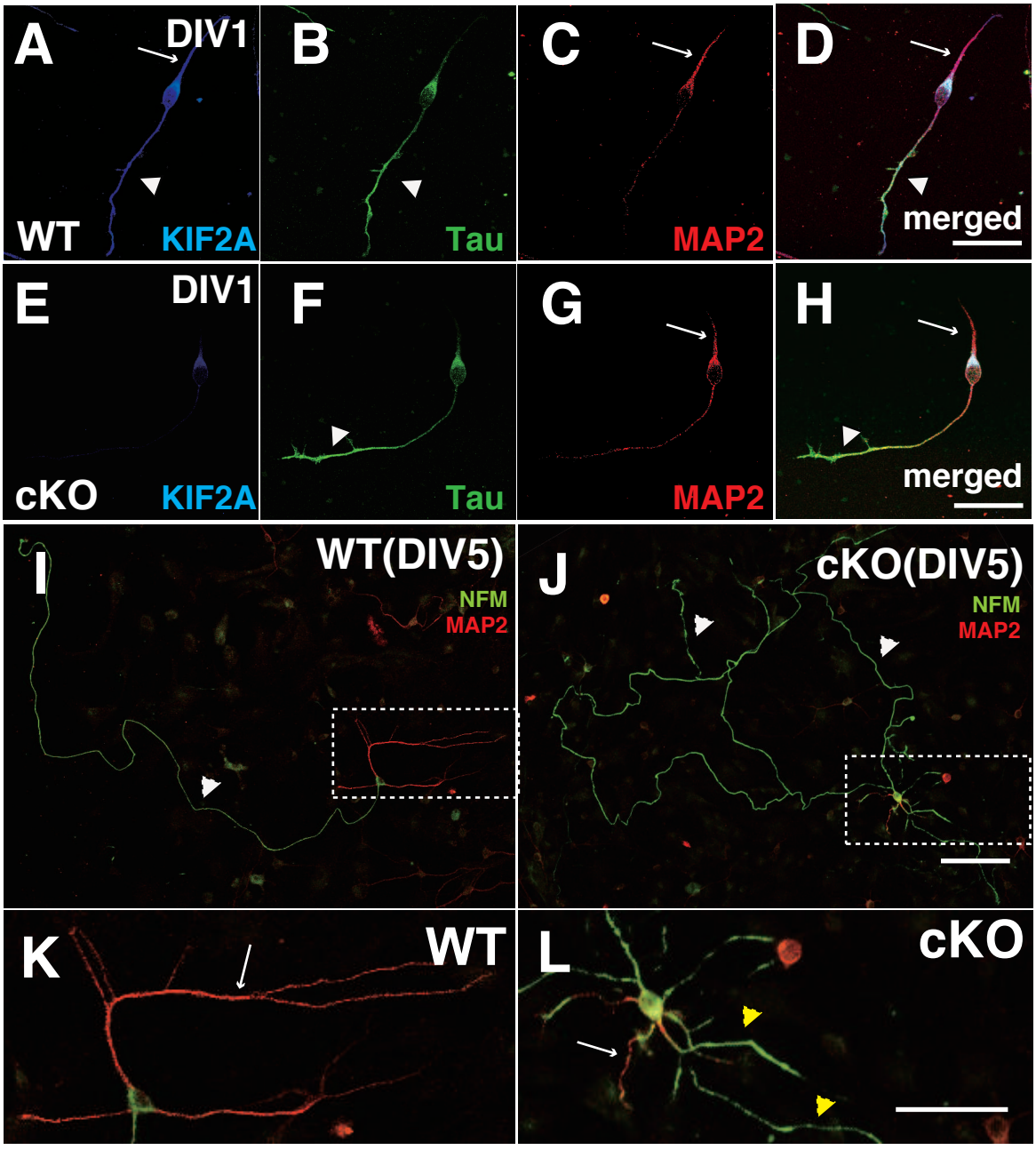
A
DIV1
WT
KIF2A
B
Tau
C
MAP2
D
merged
E
DIV1
cKO
KIF2A
F
Tau
G
MAP2
H
merged
I
WT(DIV5)
NFM
MAP2
J
cKO(DIV5)
NFM
MAP2
K
WT
L
cKO

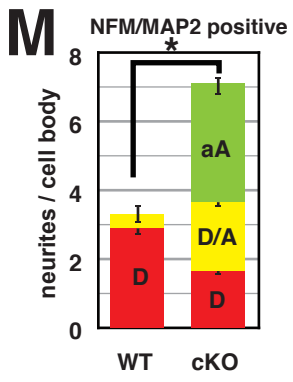
M
NFM/MAP2 positive
*
neurites / cell body
8
6
4
2
0
aA
D/A
D
D
WT
cKO

Figure 6-figure supplement 1

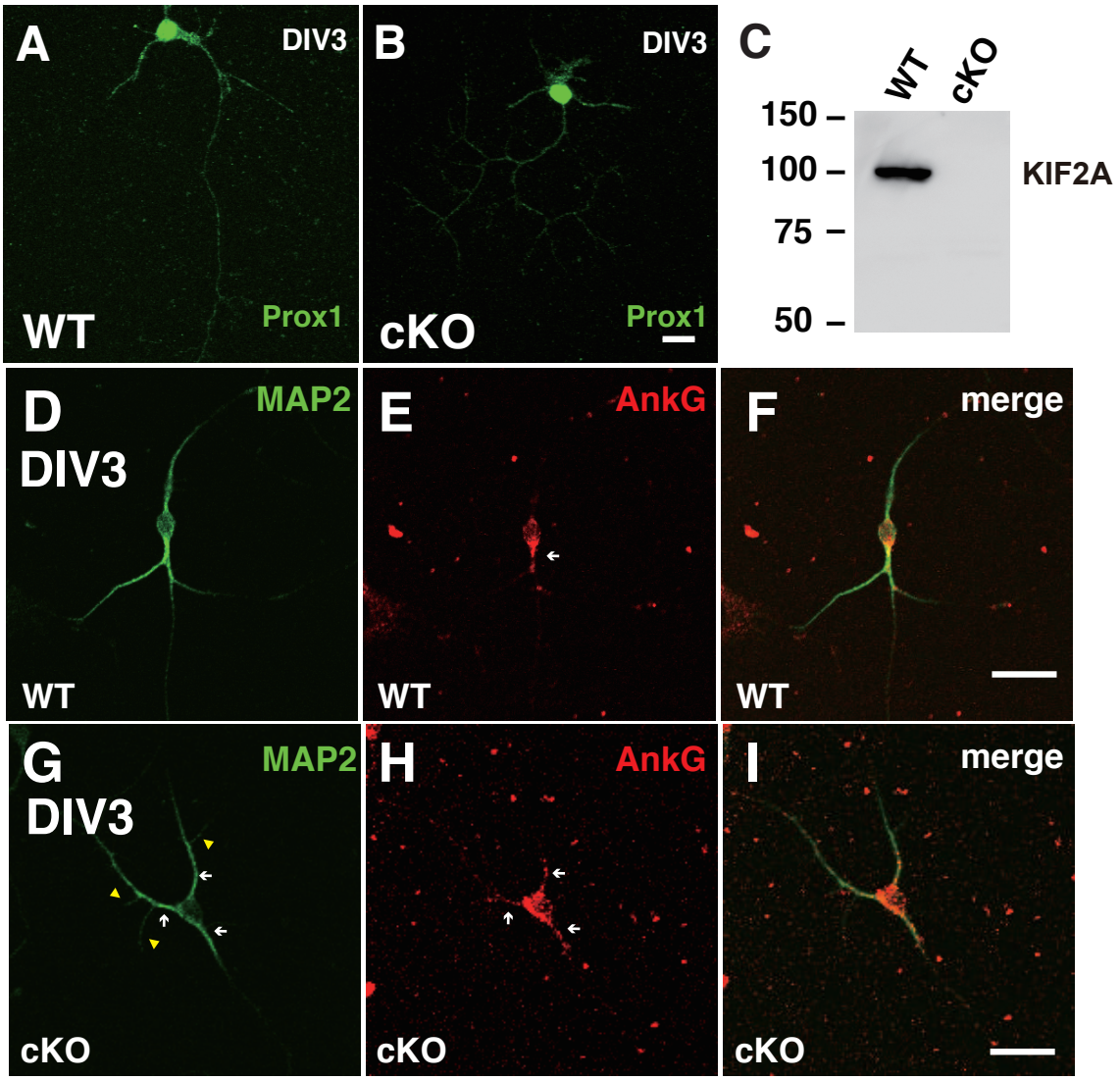

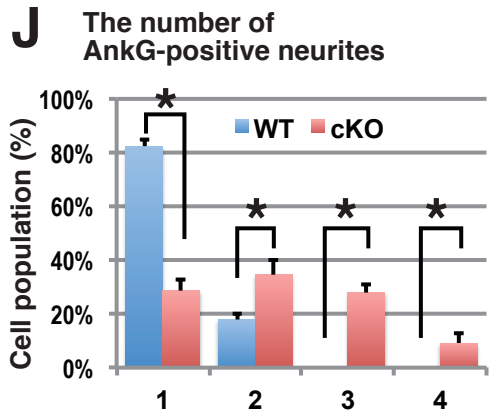

Figure 6-figure supplement 2

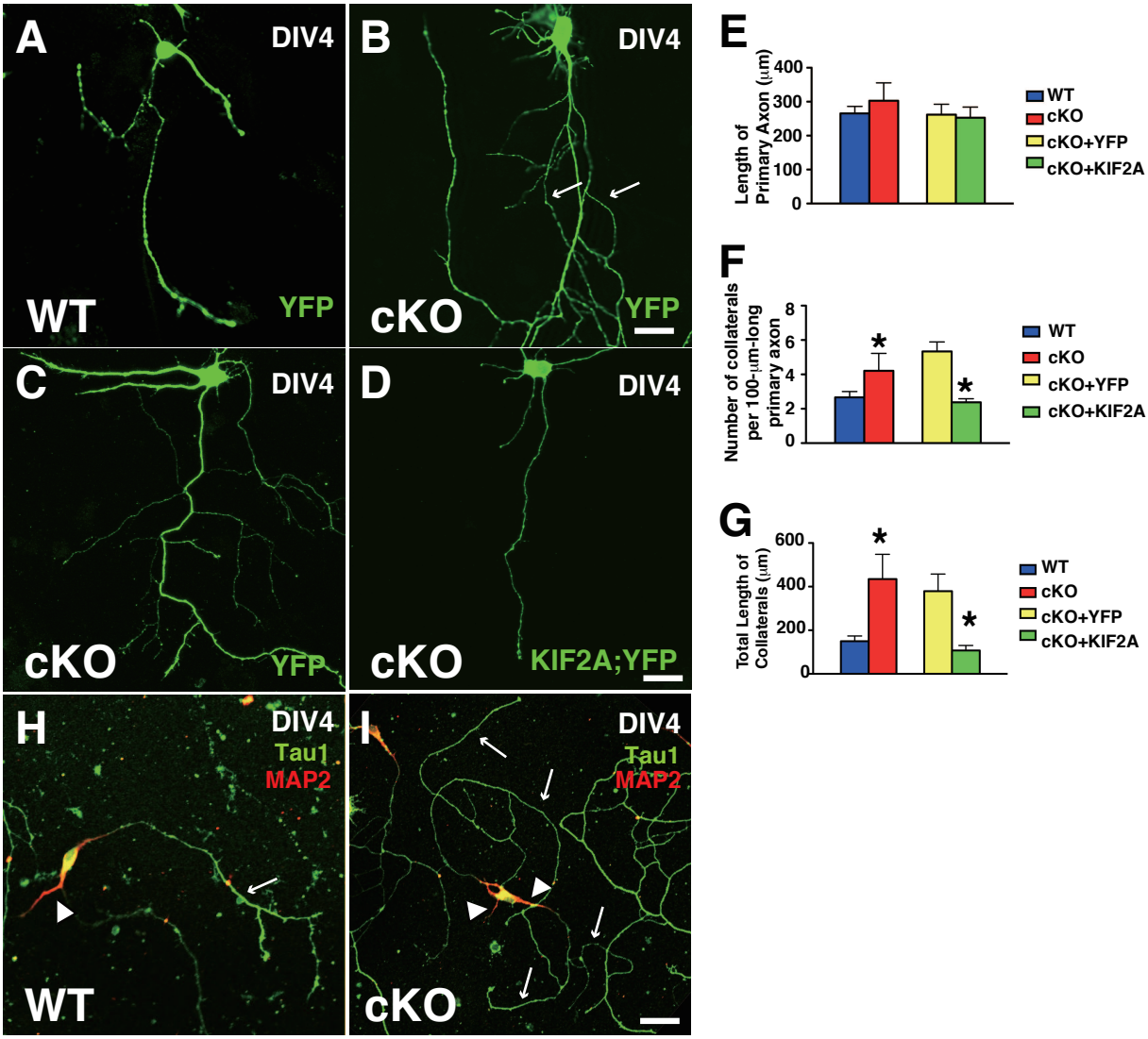

Figure 7

A.KIF2A Function in DGC development

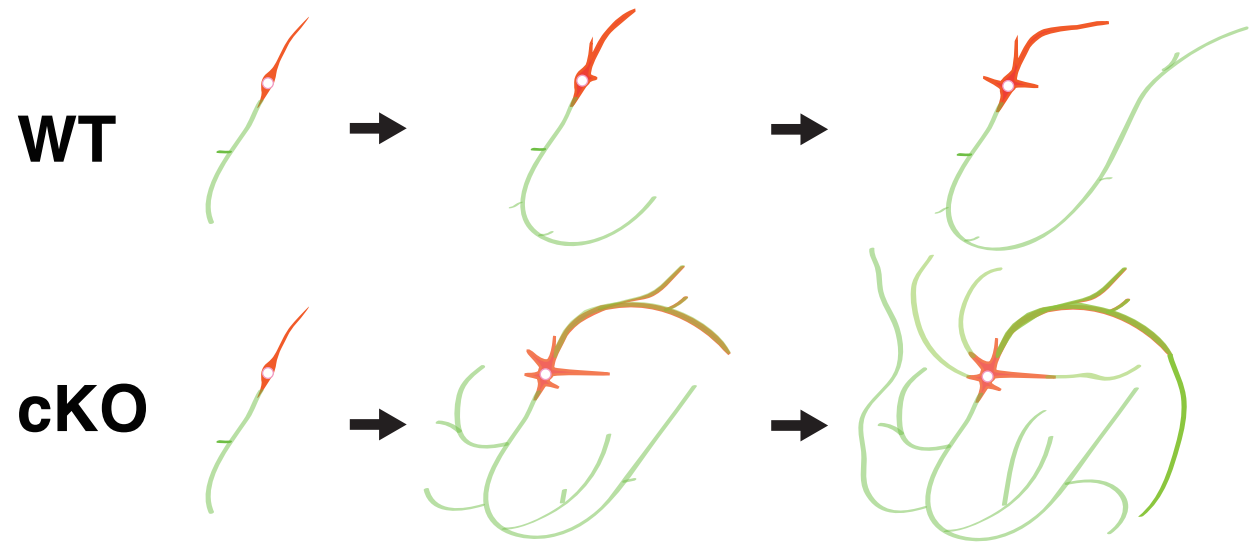

B. Contribution of postnatal KIF2A loss to hippocampal wiring and epilepsy